JOURNAL OF GEOPHYSICAL RESEARCH, VOL. 110, C04S90, doi:10.1029/2003JC002175, 2005

Long-term sediment mobilization at a sandy inner shelf site, LEO-15

Richard Styles

Marine Science Program and Department of Geological Sciences, University of South Carolina, Columbia, South Carolina, USA

Scott M. Glenn

Coastal Ocean Observation Laboratory, Institute of Marine and Coastal Sciences, Rutgers University, New Brunswick, New Jersey, USA

Received 22 October 2003; revised 9 November 2004; accepted 28 January 2005; published 1 April 2005.

[1] Nearly 2 years of wave and current observations are used to drive a calibrated bottom boundary layer model to examine sediment transport at the Long-term Ecosystem Observatory (LEO-15) located off of the southern coast of New Jersey. The multiyear record is of sufficient resolution to categorize sediment mobilization characteristics such as storm duration, frequency of occurrence, seasonal trends, and modes of transport at this shallow water sandy site. A total of 51 sediment transport events are identified within the 2 year timeframe. Thirty-two are categorized as winter events, and wintertime sediment transport constitutes 63% of the total for the 2 year period. In nearly all cases, bed load transport dominates the suspended load. The majority of the bed load transport is onshore due to wave asymmetries that lead to higher orbital velocities during the forward half of the wave cycle. For the remainder of events a bimodal wave spectrum is suspected to reverse the orbital velocity skewness leading to offshore transport. Suspended sediment transport is primarily directed alongshore toward the southwest, consistent with current patterns during northeasters. By including bed load transport, the net sediment transport for the 2 year period is directed primarily onshore and slightly alongshore toward the southwest.

Citation: Styles, R., and S. M. Glenn (2005), Long-term sediment mobilization at a sandy inner shelf site, LEO-15, *J. Geophys. Res.*, *110*, C04S90, doi:10.1029/2003JC002175.

1. Introduction

[2] It is well known that winter storms are the primary cause of sediment resuspension and transport on the continental shelf. Data obtained by *Drake and Cacchione* [1985] and *Cacchione et al.* [1987] during a winter deployment off the northern California coast in 85 m of water indicated that four storms with a combined duration of approximately 12 days were responsible for between 30% and 50% of the annual sediment transport. In this same region, *Sherwood et al.* [1994] measured bottom currents and light transmission through the 1990–1991 winter storm season. In conjunction with NOAA buoy data to estimate the wave velocities, they identified a total of 16 sediment transport events. While only two events were characterized as local, they were responsible for over half of the seasonal net transport. Their evidence indicates that local storms associated with southerly winds (downwelling favorable) likely dominate the seasonal transport for this energetic shelf region. *Ogstron and Sternberg* [1999] collected wave, current and light transmission data over a 1 year period on the northern California shelf to investigate annual sediment transport on an event-by-event basis. They identified 41 distinct sediment transport events with an average duration of 3.1 days. Three energetic winter storms were responsible for 73% of the alongshore transport but only 10% of the cross-shore transport. These event studies document the importance of combined waves and currents in driving sediment transport patterns for a narrow, steeply sloping continental shelf associated with an active-type continental margin.

[3] Less well understood are interannual variations and the corresponding potential for summer storms to mobilize and transport bed material. This is mainly due to a lack of measurements with sufficient duration to capture less frequent summer storms. Sediment transport studies aimed at examining interannual variability have been carried out mainly on the west coast of the United States [*Harris and Wiberg*, 1997]. *Harris and Wiberg* [1997] utilized NOAA buoy data to compute the near-bed wave velocities and seasonal measurements to develop probability models of near-bottom currents to predict long-term trends of sediment mobilization. Their work represents one of the first attempts to characterize long-term (multiyear) sediment transport patterns for a storm-driven continental shelf. They noted that their probabilistic approach tends to underestimate net transport because of the episodic nature of real transport events and that the most reliable methods to model sediment transport involve direct observations of waves and near-bed currents.

0148-0227/05/2003JC002175$09.00

[4] The driving force behind sediment mobilization on open coasts is near-bed orbital velocities produced by energetic surface gravity waves [e.g., *Smith*, 1977; *Grant and Madsen*, 1979; *Wiberg and Smith*, 1983]. Particle displacement consists of nearly closed orbital paths resulting in very little net suspended sediment transport. Net transport, then, is considered primarily to be due to low-frequency currents, which advect the wave-induced suspended load [*Wiberg and Smith*, 1983; *Grant and Madsen*, 1986; *Glenn and Grant*, 1987]. Another important mode is wave-forced bed load transport. In shallow water with weakly nonlinear waves, larger wave orbital velocities during the forward half of the wave cycle tend to increase the instantaneous shear stress resulting in net forward movement of sediment through ripple migration [*Traykovski et al.*, 1999]. In fact, *Traykovski et al.* [1999] presented model evidence indicating wave-forced bed load transport is as at least important as suspended load transport. If the wave spectrum is also bimodal, consisting of both low-frequency swell and high-frequency storm waves, then wave skewness may become negative resulting in offshore ripple migration [*Crawford and Hay*, 2003]. With the understanding that bed load may make a substantial contribution on sandy shelves and that waves can transport material offshore as well as onshore, a more comprehensive description of net sediment transport is achieved when both suspended and bed load phases are jointly considered.

[5] The Middle Atlantic Bight (MAB) located off of the east coast of the United States is characterized as a broad gently sloping shelf with a bed composed of primarily sandy sediments [*Swift and Field*, 1981]. Throughout the summer and fall, tropical storms in the Atlantic Ocean form a significant source of long-period swell and energetic winds (J. T. Kohut et al., Inner shelf response to tropical storm Floyd, submitted to *Journal of Geophysical Research*, 2004). Often, the inner New Jersey shelf experiences only the long-period swell as most tropical storms track farther out to sea [*Traykovski et al.*, 1999] or make landfall farther south. Under these conditions, large near-bed orbital velocities are accompanied by relatively weak local currents. In the winter, northeasters produce high local winds and large wave heights, so that strong alongshore currents coexist with energetic near-bed orbital velocities [*Wright et al.*, 1994; *Madsen et al.*, 1993]. There have been a number of studies of sediment transport during storms and fair weather conditions on the inner shelf of the MAB [*Wright et al.*, 1991; *Madsen et al.*, 1993; *Wright et al.*, 1994; *Traykovski et al.*, 1999; *Styles and Glenn*, 2002; *Harris et al.*, 2003]. In these studies, field measurements were acquired for periods of only a few months. As a result, little information has been obtained regarding the frequency of occurrence, duration and interannual budgets of sediment transport associated with long-term wave and current forcing in the MAB.

[6] In this study we utilize nearly 2 years of near-bed wave and current measurements to drive a one-dimensional (1-D) bottom boundary layer model (BBLM) to investigate interannual variations in storm-forced sediment transport at the Long-term Ecosystem Observatory (LEO-15) [*von Alt and Grassle*, 1992; *Glenn et al.*, 2000]. Given the available long-term observations, the purpose of this paper is to highlight important sediment transport characteristics such as event duration, net transport, seasonal trends and mode of transport (bed load versus suspended load). After presenting the calibration of the sediment transport algorithms and the long-term data set, model results are examined. Specific results that are relevant to long-term transport predictions are discussed followed by a narrower focus on the mechanisms driving cross-shore transport.

2. Model Calibration

[7] Sediment transport studies are often site specific so that it is standard practice to calibrate sediment transport algorithms on the basis of local wave and current forcing and knowledge of seabed morphology. A commonly used method to model sediment resuspension in continental shelf environments is to prescribe the concentration near the bed in terms of a reference value that is a function of the excess shear stress based on skin friction [*Smith and McLean*, 1977]. We adopt the following modified form of the *Smith and McLean* [1977] reference concentration model noting that it must be calibrated for the wave-dominated sandy LEO-15 site:

$$
\begin{aligned}
C(z_0) &= c_b \gamma_0 \left(\frac{\psi'}{\psi_c} - 1 \right) && \psi' > \psi_c \\
C(z_0) &= 0 && \psi' \leq \psi_c,
\end{aligned}
\tag{1}
$$

where $C(z_0)$ is the time-averaged reference concentration evaluated at z_0, z_0 is the hydraulic roughness, c_b is the bed concentration, γ_0 is the resuspension coefficient, ψ' is the magnitude of the Shields parameter based on skin friction over a wave period and ψ_c is the critical shear stress for the initiation of sediment motion. The Shields parameter is related to the bottom wave orbital velocity, u_b, through a quadratic drag law

$$
\psi' = \frac{1/2 f_w \left(\sqrt{2} u_b^2 \right)}{(s-2) g d_{\mathrm{med}}},
\tag{2}
$$

where the friction factor based on the grain roughness is defined by

$$
f_w = \exp\left[5.61 \left(\frac{A_b}{d_{\mathrm{med}}} \right)^{-0.109} - 7.30 \right]
\tag{3}
$$

[*Madsen*, 1994], and d_{med} is the median grain diameter (=0.04 cm), A_b is the near-bed excursion amplitude, s is the relative sediment density (=2.65), and g is the acceleration due to gravity. The $\sqrt{2}$ modification to u_b gives a better representation of the Shields parameter when compared to sediment concentration measurements at LEO-15 [*Traykovski et al.*, 1999]. In all calculations, u_b is the equivalent wave orbital velocity as defined by *Madsen et al.* [1988]. Equation (1) is modified from the original *Smith and McLean* [1977] formulation in three ways. Firstly, their model was for currents, whereas we are applying it to combined flows. *Grant and Madsen* [1982] showed that the sediment response time is much less than the wave period for most continental shelf applications. This allowed *Glenn and Grant* [1987] to reason that the above formulation is applicable to combined wave and current flows. Secondly,

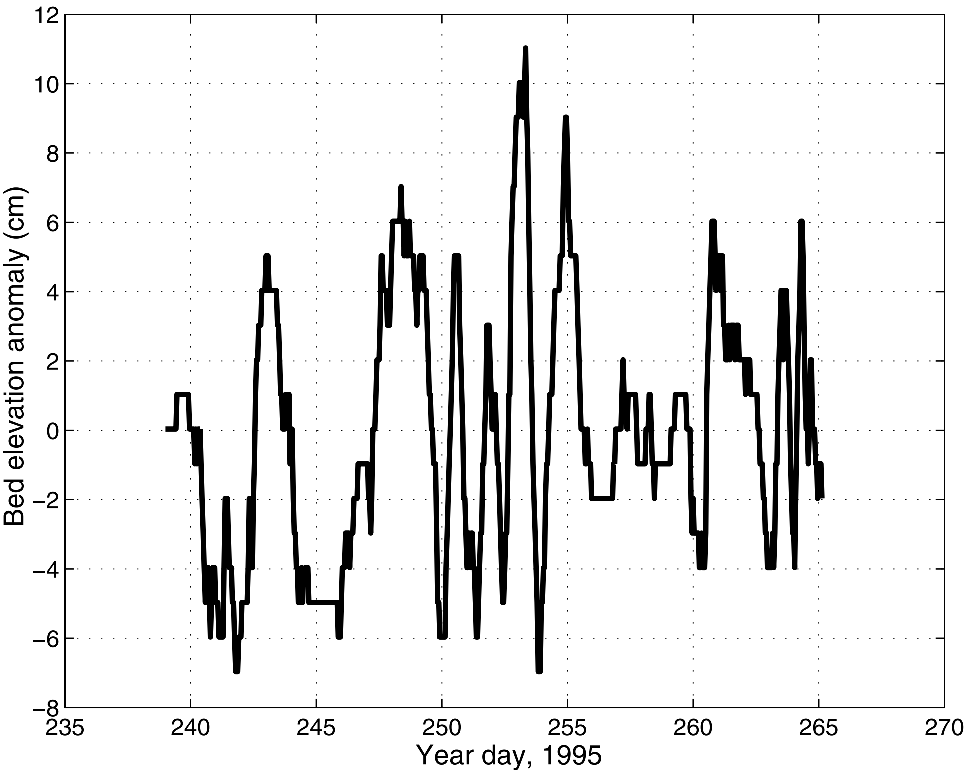

Figure 1. Bed elevation anomaly computed from the Acoustic Backscatter System (ABSS). Positive values indicate that the instantaneous bed elevation directly below the sensor is greater than the average for the 6 week period.

Smith and McLean [1977] divided (1) by the term $[1 + \gamma_0((\psi^t/\psi_{cr}) - 1)]$ to insure that the reference concentration never exceeds the concentration in the bed. *Wikramanayake and Madsen* [1992] showed that under most conditions on sandy continental shelves, this term is small and can be neglected. Thirdly, (1) is based on the wave-averaged orbital velocity, whereas *Glenn and Grant* [1987] integrated the instantaneous wave velocity over a wave period. Because we are using the equivalent wave orbital velocity, rather than an integrated value, the reference concentration model must be calibrated.

[8] A 6 week observational study was conducted in August–September 1995 that produced high-resolution suspended sediment concentration, current and wave measurements at LEO-15. The field program and measurements have been described by *Traykovski et al.* [1999] and *Styles and Glenn* [2002]. Two large wave events and an additional period of heightened swell activity associated with distant tropical storms generated bottom shear stresses large enough to resuspend bed sediments throughout most of the 6 week period. Suspended sediment concentration data were obtained using a downward looking Acoustic Backscatter System (ABSS) that profiled the lower ~1 m of the water column in 1 cm bins [*Traykovski et al.*, 1999]. *Traykovski et al.* [1999] measured the median grain diameter at LEO-15 to be 0.04 cm, which is the size they used to calibrate the ABSS. Wave and current measurements were obtained from a BASS (Benthic Acoustic Stress Sensor) array [*Styles and Glenn*, 2002]. Burst averaged concentration profiles were computed along with hourly wave measurements to produce a time series of sediment concentration and ψ'.

[9] Because the purpose here is to examine sediment transport, the vertical distribution of individual profiles is less important than the integral of the suspended load over the near-bed region where concentrations are greatest. Depth-integrated concentration (C_d) was computed using the trapezoidal rule by integrating the ABSS profiles. Peter Traykovski (personal communication, 2000) has noted that the ABSS is not consistently accurate to within about 6 cm from the bed in the presence of wave-generated ripples because the width of the ABSS footprint can be on the same order as the ripple wavelength. Depending on what section of the ripple is directly underneath the beam, some portions of the lower few ABSS bins are sampling both suspended sediments and the bottom. This produces anomalously high acoustic return intensities that do not accurately reflect the suspended sediment concentration. As such, two procedures are used to define the lower integration limit. If the local bed height (the height measured by the ABSS for any given burst) is less than the average bed elevation for the 6 week period, then the concentration is integrated from 6 cm above the ripple height, as determined by *Traykovski et al.* [1999], to 80 cm above the bed (Figure 1). If the local bed height is greater than the average, then the concentration is integrated from 6 cm above the local bed height to 80 cm. This course of action ensures that all measurements are high enough above the uneven bottom to produce accurate suspended load estimates yet low enough that most of the transport is sampled. The relatively high settling velocity for the medium

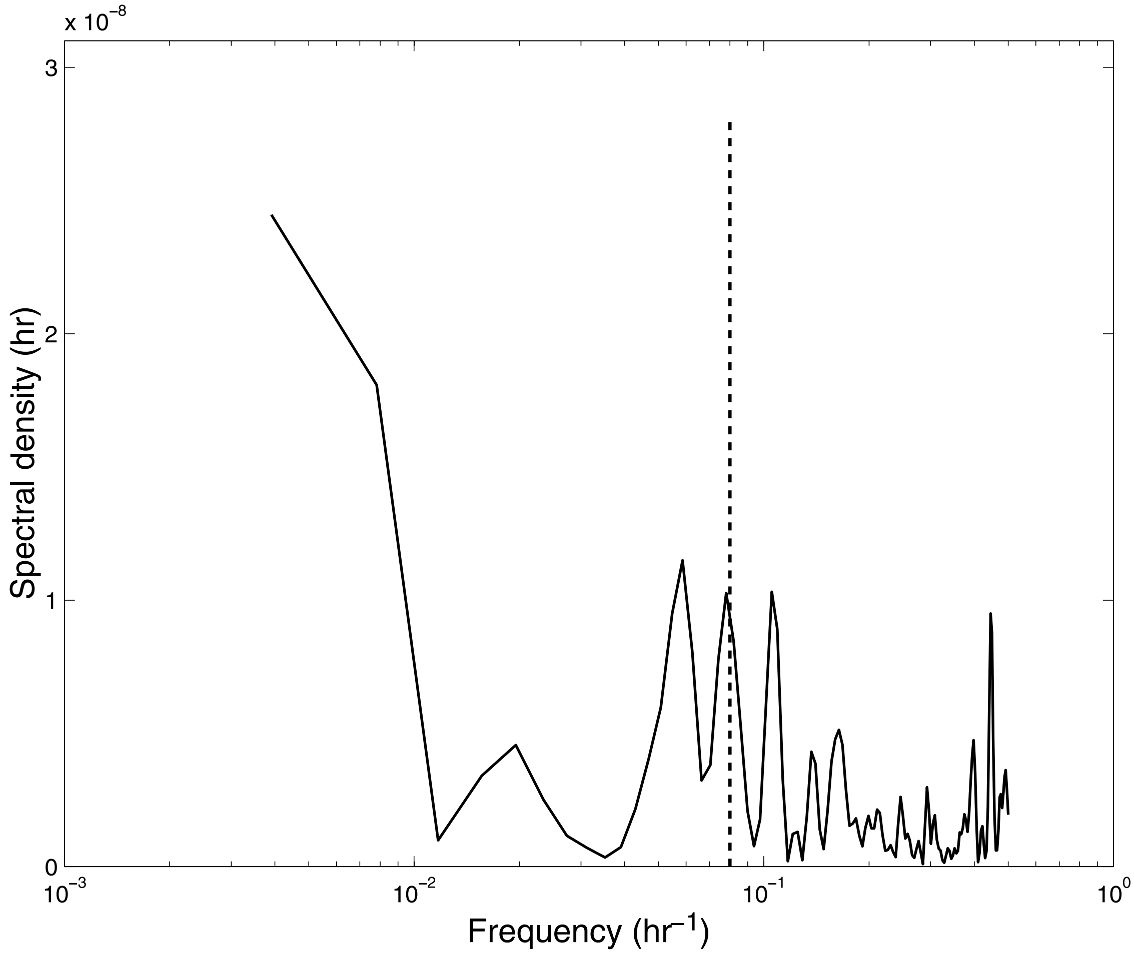

Figure 2. Spectral density function for the depth-integrated suspended sediment concentration obtained from the ABSS. The vertical dashed line denotes the semidiurnal tidal period.

sized sand found at the study area means that the majority of the suspended load is confined very near the bed. Therefore concentrations above about half a meter are an order of magnitude lower than within a few centimeters of the bed and will not contribute significantly to the integral.

[10] The spectral distribution of the depth-integrated concentration reveals a peak near the same frequency as the M2 tidal constituent (Figure 2). Maximum near-bed tidal currents are on the order of 5 cm/s at LEO-15 and are incapable of resuspending the medium to coarse sandy sediment [*Styles and Glenn*, 2002]. Storm-driven transport is associated with episodic frontal systems that are typically longer and uncorrelated with the semidiurnal tidal period. In order to isolate the storm-driven component, the depth-integrated concentration is run through a 36 hour low-pass filter to remove the tidal signal. The concentration profile and its depth-integrated value are dependent on γ_0 through the reference concentration. The parameter γ_0 is calibrated by minimizing the relative difference between modeled and measured depth-integrated transport for the full 6 week record. Model estimates are determined from the neutral version of the *Styles and Glenn* [2000, 2002] BBLM. The model features a continuous eddy viscosity profile and computes the combined wave and current shear stress for a noncohesive sediment bed. Model inputs include the near bottom wave orbital velocity, wave excursion amplitude, the mean current at a selected height off of the bottom and the angle between the wave and current [*Grant and Madsen*, 1979; *Styles and Glenn*, 2000]. Concentration profiles are computed based on the *Styles and Glenn* [2000] model and the reference concentration is determined from (1). For the calibration, a single grain size class of 0.04 cm is used.

[11] Using measured wave and current data from the deployment to drive the model, concentration profiles are computed for each hour. These modeled profiles are then integrated over the same range as the ABSS measurements. The reference concentration is then back calculated by adjusting γ_0 until the model matches the measurements. The primary interest is to study the total sediment transport over events, so that the calibration statistic is determined as the difference between the total measured depth-integrated concentration and the model over the 6 week deployment. A relative difference of zero was found when $\gamma_0 = 4.0 \times 10^{-4}$.

[12] Figure 3 depicts the current, wave and suspended sediment concentration data used to calibrate the reference concentration model. Sediment resuspension is clearly linked to waves and the overall comparison of the modeled depth-integrated concentration to the measurements is reasonable. The model tends to overestimate (underestimate)

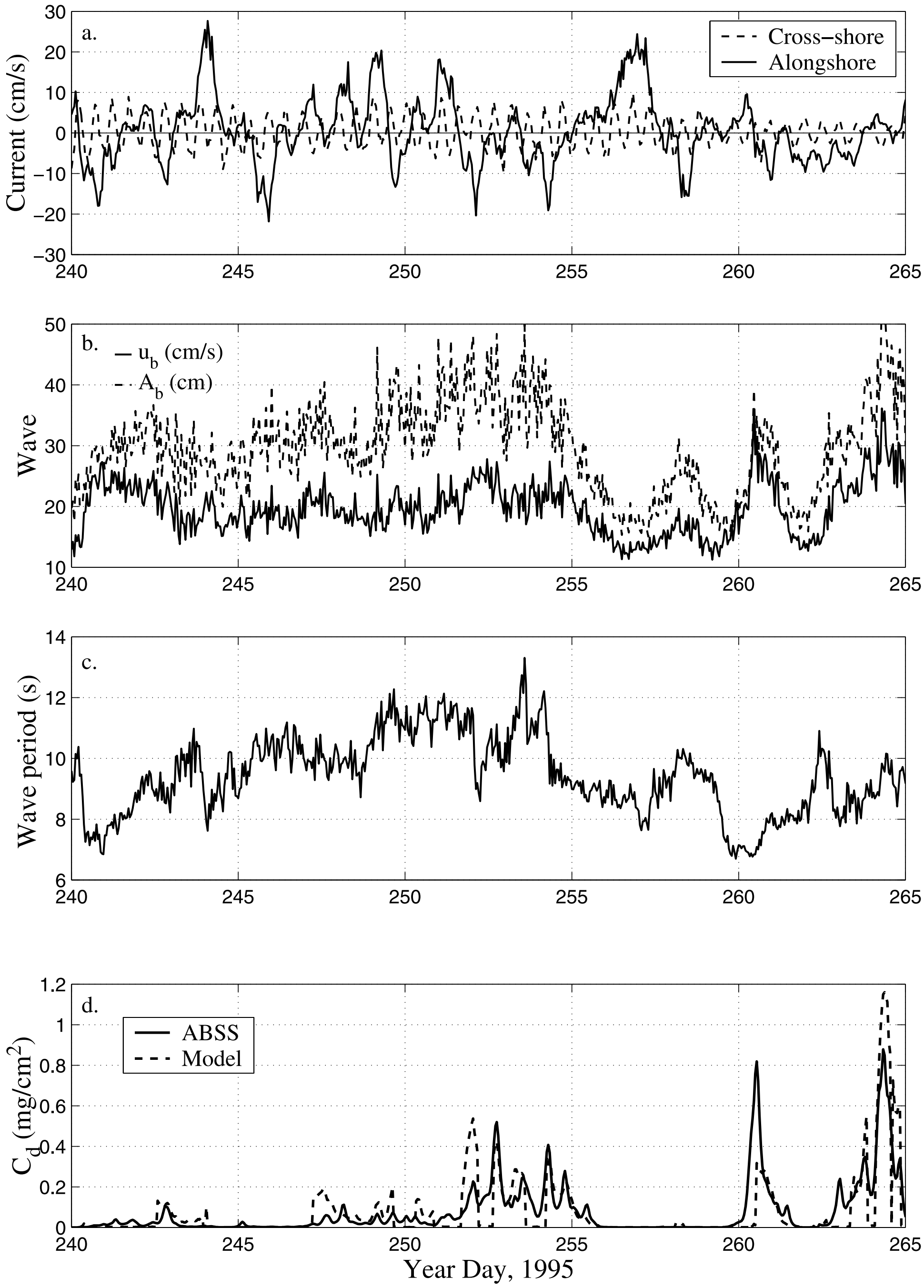

Figure 3. Time series of (a) current, (b) wave orbital velocity and wave excursion amplitude, (c) wave period, and (d) measured and computed depth-integrated suspended sediment concentration used to calibrate the resuspension coefficient.

the concentration for the period centered on year day 264 (261). Examination of the wave orbital velocities for the period centered on year day 261 indicate that they are as energetic as other time periods that show higher concentration levels. Since the reference concentration and the majority of the upward turbulence sediment flux are controlled by the waves, one would expect the model to predict higher concentrations during this time period. However, the upward turbulent flux is also dependent on the length scales that define the flow. The most important scale is the wave boundary layer thickness, since it is within the wave boundary layer that the highest concentrations are predicted [*Styles and Glenn*, 2000]. If it is small then most of the suspended load is maintained near the bed and the model will predict lower overall depth-integrated concentrations. The period centered on year day 261 has relatively high u_b values but it also has the shortest wave period. For a given shear stress, a shorter wave period leads to a reduction in the thickness of the wave boundary layer [*Grant and Madsen*, 1979]. This in turn reduces the total amount of sediment in suspension and explains why the model underestimates the depth-integrated concentration. For the period centered on

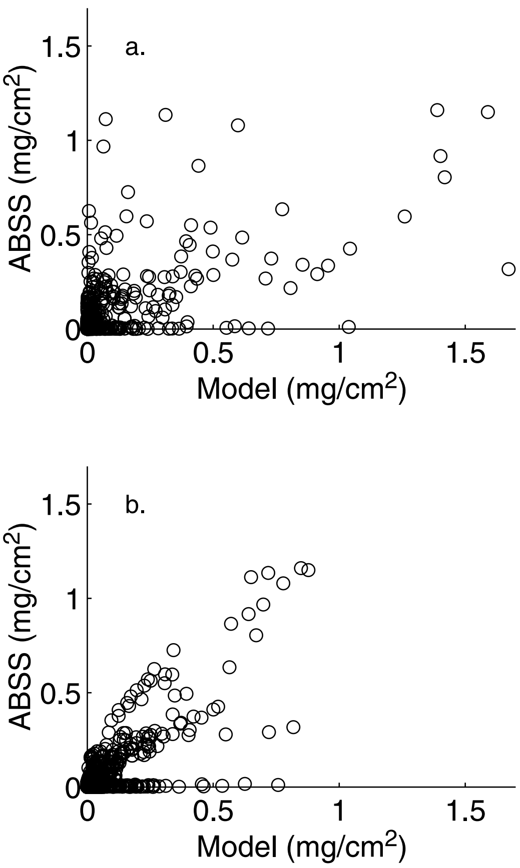

Figure 4. Scatterplot depicting the relationship between measured and modeled depth-integrated sediment transport: (a) unfiltered and (b) filtered.

year day 264, the difference between measured and modeled depth-integrated concentration is less than a factor of 2. *Traykovski et al.* [1999] noted that for the 0.04 cm grains found at LEO-15, the accuracy of the ABSS in computing sediment concentration is within about a factor of 2. Therefore our comparison to measured values is consistent with the relative accuracy of the method chosen to extract concentration estimates from acoustic backscatter.

[13] Figure 4 is a scatterplot of measured versus predicted depth integrated sediment concentration for both the filtered and nonfiltered data sets. The filtered data ($r^2 = 0.58$) shows better agreement with the model than the unfiltered ($r^2 = 0.35$) and explains why we chose to filter the data set to remove the tidal component.

[14] As mentioned above, the lower integration limit of approximately 6 cm above the bed is constrained due to unavoidable inaccuracies in the suspended sediment concentration measurement. Because most of the suspended load occurs in the energetic thin wave boundary layer, there is the potential that the calibration procedure is missing a good portion of the high concentration suspended sediment. Wave boundary layer thickness is usually scaled as $\kappa u_{*cw}/\omega$, where κ is von Karmans constant (0.4), u_{*cw} is the maximum combined wave and current shear velocity and ω is the wave radian frequency [*Grant and Madsen*, 1979]. However, in the presence of roughness elements with dimensions that are on the order of the wave excursion amplitude, this estimate of wave boundary layer thickness tends to be too low [*Davies and Villaret*, 1998]. *Mathisen and Madsen* [1996a, 1996b] conducted flume experiments with triangular bars that approximate the shape of 2-D ripples and found that the wave boundary layer thickness was more closely related to ripple dimensions, i.e., $\delta_{cw} \approx 4\eta$, where η is ripple height. In the *Styles and Glenn* [2000] version of the *Grant and Madsen* [1979] model, which is the one used in the present study, δ_{cw} is related to the scale height $z_2 (=\alpha\kappa u_{*cw}^2/u_{*c}\omega)$, where u_{*c} is the time average of the shear stress over a wave period and α is an internal model closure constant [*Styles and Glenn*, 2002]. Figure 5 depicts estimates of wave boundary layer thickness for the 6 week deployment using the *Mathisen and Madsen* [1996a, 1996b] results and z_2 from the *Styles and Glenn* [2000] model. In both cases, wave boundary layer thickness is almost always greater than 6 cm and shows that the integration limits imposed by the ABSS are still able to capture a significant fraction of the modeled outer wave boundary layer. Compared to most of the other sediment transport time periods, estimates based on ripple height are relatively low around year day 260. This is the same time period that the model underestimated the depth-integrated concentration and further supports our assumption that reduction in the modeled wave boundary layer thickness due to the shorter waves leads to lower modeled sediment resuspension.

[15] Bed load transport is computed using the Meyer-Peter and Muller formula as modified by *Madsen and Wikramanayake* [1991] for combined wave and current flows. The bed load module expresses the transport as a nonlinear function of the excess shear stress based on skin friction, i.e.,

$$\begin{aligned} Q_b &= 8\left(\frac{\psi^{it}}{\psi^{c}} - 1\right)^{1.5} \sqrt{(s-1)gd}\,d\left(\hat{i} + \hat{j}\right) \qquad && \psi^{it} > \psi_c \\ Q_b &= 0 && \psi^{it} \leq \psi_c, \end{aligned} \tag{4}$$

where ψ^{it} is the instantaneous Shields parameter and $\hat{i}$ and $\hat{j}$ are unit vectors in the cross- and alongshore directions, respectively. The instantaneous Shields parameter is determined using (2) but with u_b replaced by the instantaneous near-bed wave velocity. The friction factor is computed as above using the spectrally averaged excursion amplitude (A_b). This model is chosen because *Traykovski et al.* [1999] noted that it compared favorably to their estimates of bed load transport via ripple migration at LEO-15.

3. Long-Term Measurements

[16] In accordance with the long-term monitoring strategy, a pair of S4 current meters was deployed at LEO-15 for a period of approximately 2 years beginning in 1994. Because one of the primary goals was to obtain wave and current data to drive bottom boundary layer models, both S4s were programmed to sample at 2 Hz for an 18 min burst each hour. To provide optimal long-term coverage, the S4s were deployed in series at Node A (74.26°W–39.46°N) (Figure 6). Each unit operated for approximately 2 months and was then recovered for servicing and replaced by its sister unit. Initially, the S4s were placed at a height of 2 m off of the bottom. In October 1994, the height of the sensors was

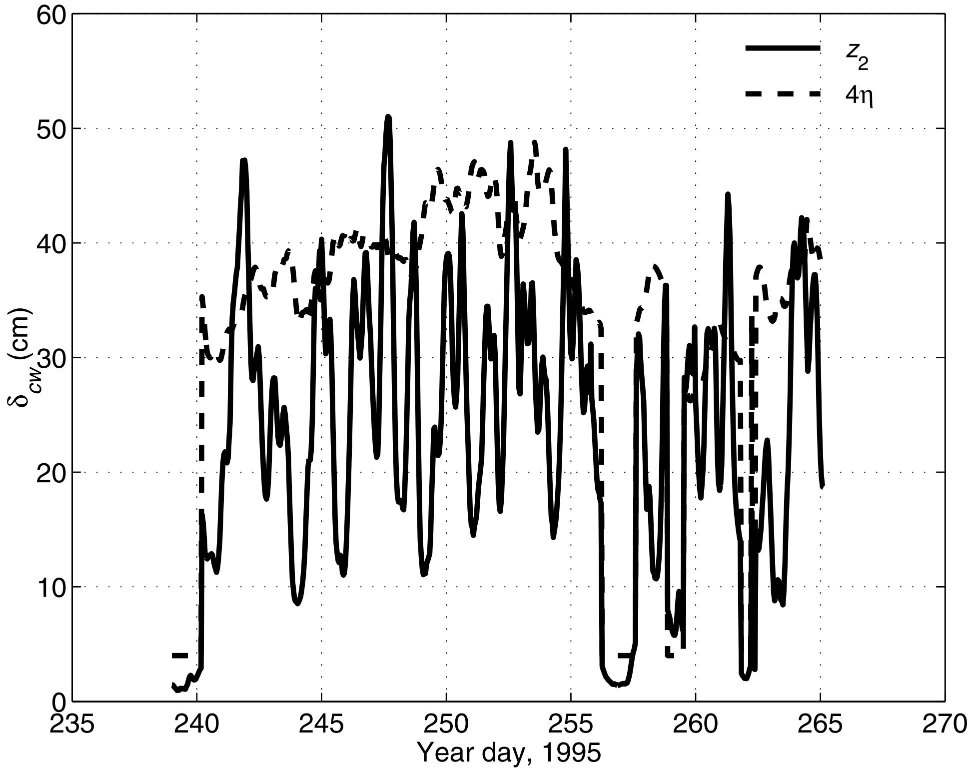

Figure 5. Model estimates of the wave boundary layer thickness.

lowered to 1 m to accommodate a more robust mooring system.

[17] The 1/2 s pressure record from each burst was fast Fourier transformed and converted to the near-bottom orbital velocity spectrum, which was then converted into the equivalent near-bottom wave orbital velocity, u_b, [*Madsen et al.*, 1988]. The equivalent wave radian frequency, ω_r, was computed as described by *Styles and Glenn* [2002] and the

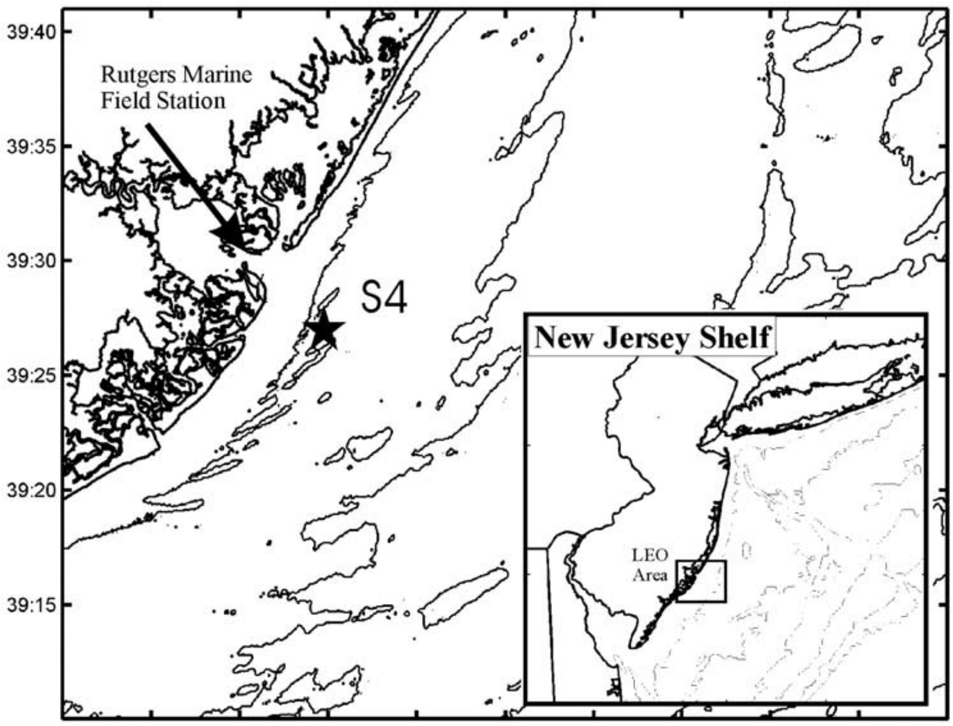

Figure 6. LEO-15 study site including the regional coastline (inset) and the location of the S4 moorings.

direction of maximum velocity variance was used to define the wave direction. The sediment parameters required as input included sediment grain size distribution, porosity and specific gravity. Surface sediment samples obtained by divers at LEO-15 in the summer of 1994 were analyzed for grain size distribution and type. The predominant sediment type was noncohesive medium sized quartz sand with a density of 2.65 g/cm^3 and a median grain diameter of 0.04 cm. The bed concentration, c_b, was set equal to 0.65. Because the model is calibrated using 0.04 cm sand, this will represent the grain diameter for all calculations.

[18] The near-bed wave velocities required to drive the bed load transport model were computed from the instantaneous horizontal velocity components. Each component was high-pass filtered with a cutoff of 20 s to remove infragravity motions [*Traykovski et al.*, 1999]. The filtered components were input into the bed load transport model and the net transport for each hour was computed as the sum of the instantaneous values.

[19] The primary function used here to describe sediment mobilization at LEO-15 is the depth-integrated sediment transport defined as

$$Q_s = \int_{z_0}^{h} C(z)u(z)dz, \tag{5}$$

where h is the water depth, u is the modeled current and C is the modeled concentration. Another important variable to described sediment transport in terms of individual events is the total depth-integrated sediment transport defined by

$$Q_{st} = \int_{T_0}^{T_e} Q_s(t)dt \tag{6}$$

for the suspended load and

$$Q_{bt} = \int_{T_0}^{T_e} Q_b(t)dt \tag{7}$$

for the bed load, where T_0 and T_e denote the beginning and end of an event. The integrals are computed using the trapezoidal rule [*Atkinson*, 1989]. Within each event, Q_s and Q_b will take on maximum values denoted Q_{sm} and Q_{bm}, respectively. Concentrations are expressed in terms of a volume fraction (i.e., liters per liters or cubic centimeters per cubic centimeter) of the sediment-water mixture. In all calculations, the concentration is converted to a mass fraction by multiplying by the sediment density. Concentrations are expressed in mg/cm^3, which gives the transport in units of mg/cm/s. Physically, this is the amount of sediment transported per centimeter width normal to the flow direction. The total depth-integrated transport (mg/cm) is then the total amount of sediment transported per centimeter width over the given time period.

4. Sediment Transport Event Criteria

[20] The calibrated BBLM was run for the 2 year time period using the input wave, current and sediment parameters discussed above. Sediment resuspension is associated with higher wave-induced near-bed flow and therefore is episodic. There will be periods when the model skips through several days or even weeks before the conditions are energetic enough to remobilize the sandy bed. These will have a distribution that is based on the duration of the quiescent period separating occurrences of sediment mobilization and on the number of consecutive hours in which sediment mobilization occurs.

[21] Time series of the sediment concentration output from the model were used to identify the distribution of sediment resuspension occurrences. The results are displayed in Figure 7a. The vertical axis denotes the number of times the model predicted sediment mobilization and the horizontal axis categorizes these resuspension occurrences by duration. For example, the first vertical bar denotes the total number of occurrences whose combined total lasted 1, 2, or 3 hours. The last vertical bar denotes all occurrences with durations greater than 22 hours. When these values are weighted by the number of hours per occurrence, sediment mobilization with a duration greater than 22 hours account for the majority of sediment transporting time periods (Figure 7b). A spectral gap occurs around 15 hours separating the large-scale transport occurrences from the short-term occurrences. Using this spectral gap as a guide, a sediment transport event is defined as any period that indicates at least 15 consecutive hours of nonzero sediment in suspension. The event will further be defined as having ended when 15 consecutive hours of zero sediment resuspension is calculated by the model. This definition establishes a consistent event criterion, where, presumably, large synoptic atmospheric systems that generate strong waves and currents are considered the primary impetus for driving sediment motion on the inner shelf. Tables 1 and 2 list the number of events along with sediment transport statistics to be discussed. Twenty-five transport events were identified in 1994 and 26 were identified in 1995 with durations ranging from a minimum of 17 hours to a maximum of 421 hours (17.5 days).

5. Results

[22] The near-bed flow is composed of both low-frequency currents and waves, which combine to entrain and transport sediment. It is generally accepted that waves are responsible for initiating sediment motion on the New Jersey coast [*McClennen*, 1973]. Figure 8 shows significant wave height, H_s, calculated from the S4 pressure data and NOAA buoy 44009 located near the entrance to Delaware Bay, along with individual sediment transport events. Significant wave height exceeds ~0.5 m for all events. A number of times during the 2 year record H_s exceeds 0.5 m without a corresponding identified transport event. These represent transport occurrences that are less than 15 hours in duration and are neglected under the present event criteria threshold. However, unmistakably, transport events correspond to time periods with high waves. Episodic data gaps scattered throughout the 2 year period reflect unavoidable S4 downtime for maintenance and the commitment of these instruments to competing field experiments. These few data gaps notwithstanding, the combined S4s provide 78% coverage during the first year and 70% coverage during the second year. They also provide at least partial coverage for each season.

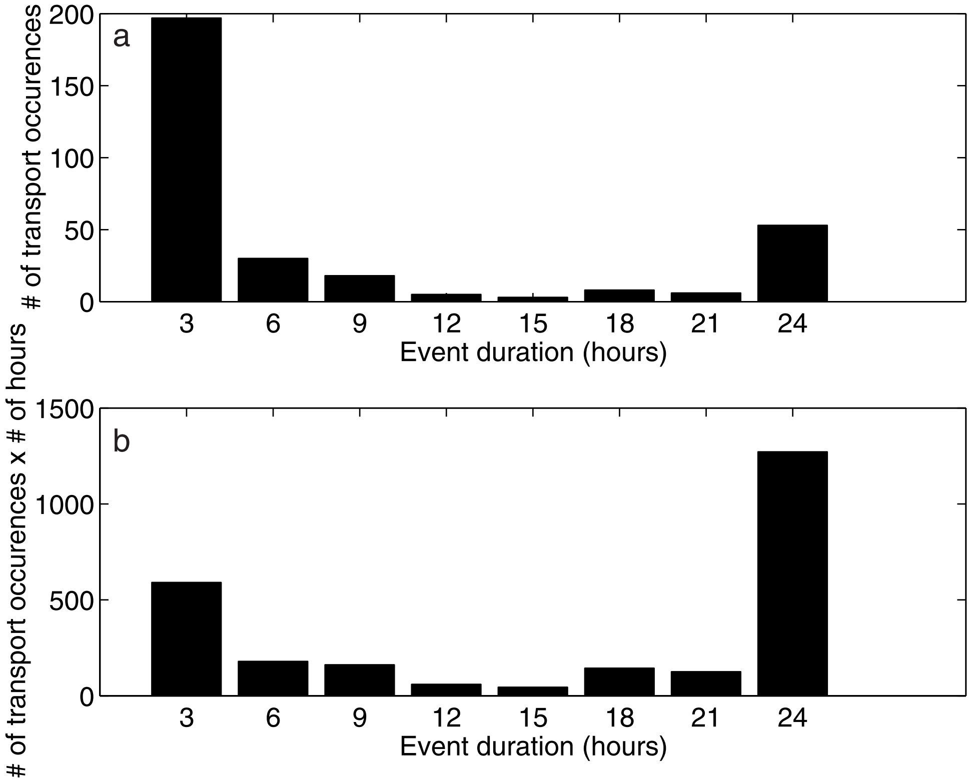

Figure 7. (a) Distribution of sediment transport occurrences for the 2 year time period. The vertical axis denotes the total number of occurrences, grouped by duration, for the corresponding temporal bands identified on the horizontal axis. For example, the number 3 on the horizontal axis represents all transport occurrences with a duration of either 1, 2, or 3 hours. (b) Similar to Figure 7a, but each occurrence is weighted by occurrence duration. All transport occurrences with a duration greater than 22 hours are grouped in the final column.

Table 1. Sediment Transport Statistics for 1994 Events[a]

Event	Date (1994)	Event Duration, hours	Cross Shore, mg/cm		Alongshore, mg/cm		Maximum, mg/cm/s		Total Depth-Int., mg/cm	
			B	S	B	S	B	S	B	S
1	22 Feb.	81	−142.1	104.8	1147	−1332	610.0	106.2	6522	1423
2	1-Mar	77	3976	−2262	3266	−4444	1858	422.8	13023	5740
3	7-Mar	216	−474.1	−60.71	−229.4	2.962	208.8	7.630	4418	136.1
4	27-Mar	60	−559.5	−32.73	95.03	17.80	422.8	7.008	2024	61.56
5	1-Apr	73	−530.9	−10.46	−225.1	−3.463	25092	2.414	27186	21.69
6	13-Apr	94	−993.5	−24.84	515.0	2.973	117.3	2.562	2419	28.58
7	20-Apr	17	−160.1	−0.966	205.3	−0.317	80.84	0.282	471.1	1.284
8	4-May	56	760.8	−71.38	919.6	−567.4	254.7	83.63	3044	630.0
9	8-May	20	−260.8	−0.640	246.6	−0.527	74.41	0.294	539.3	1.895
10	19-May	133	1199	6.843	103.3	−58.05	2892	6.739	6710	76.56
11	26-May	26	294.6	−2.179	−273.0	−0.589	69.87	0.874	576.0	3.071
12	22-Jul	54	234.3	−11.10	−180.4	−1.695	80.86	1.792	497.8	11.73
13	28-Jul	33	107.8	−3.977	−40.33	−0.987	27.20	0.671	207.6	4.442
14	6 Aug.	40	−352.3	−0.143	−60.60	−12.57	192.2	1.860	819.0	16.08
15	14 Aug.	43	−196.1	−5.508	259.6	−1.772	69.03	1.160	888.3	6.966
16	18 Aug.	30	−368.3	−3.828	270.2	−2.431	50.63	1.447	562.6	4.867
17	22 Aug.	79	−61.54	77.04	678.5	−533.9	1937	93.56	3527	548.4
18	4 Sept.	63	685.6	21.37	459.5	−201.8	321.2	16.76	1868	211.7
19	15 Oct.	154	−1592	−6.765	−97.32	−532.3	276.2	66.98	4584	561.1
20	1 Nov.	32	−252.6	−9.993	−54.13	22.34	62.73	5.585	556.3	32.78
21	16 Nov.	157	−1594	−45.75	603.4	−702.1	900.8	39.10	9075	848.1
22	27 Nov.	65	−641.8	−35.35	−458.2	252.4	17734	33.73	21413	273.5
23	5 Dec.	21	−26.85	−2.681	9.605	3.363	2709	1.103	3107	5.433
24	10 Dec.	230	−2758	186.7	−323.5	−756.3	189.5	24.51	8229	858.8
25	23 Dec.	72	−2848	401.7	161.6	−2322	550.4	276.7	5264	2400
Annual totals		**1926**	**−6554**	**−1793**	**6998**	**−11172**	**56781**	**1205**	**127531**	**13908**

[a]Symbols are defined in the text. B, bed load; S, suspended load.

Table 2. Sediment Transport Statistics for 1995 Events[a]

Event	Date (1995)	Event Duration, hours	Cross Shore, mg/cm		Alongshore, mg/cm		Maximum, mg/cm/s		Total Depth-Int., mg/cm	
			B	S	B	S	B	S	B	S
26	13 Jan.	210	−1934	−95.33	798.0	−54.72	357.4	25.66	8713	646.4
27	4 Feb.	23	184.8	0.771	−25.98	−144.0	353.9	17.99	1487	146.5
28	16 Feb.	46	−163.3	−12.03	−63.53	−3.104	69.50	2.451	830.0	18.16
29	19 Feb.	133	1082	32.05	212.1	0.284	39139	39.13	43106	61.91
30	26 Feb.	268	575.5	57.31	841.0	−211.6	301.4	10.13	6601	296.7
31	15-Mar	81	−588.5	5.222	−170.3	−0.448	91.80	1.371	1535	17.70
32	20-Mar	68	251.4	−2.238	29.61	−0.468	58.74	0.557	1045	7.460
33	30-Mar	47	−166.8	−0.827	−52.40	−0.148	113.6	0.611	578.8	4.336
34	9-May	85	−648.8	−13.93	76.76	−12.96	1292	4.489	3634	34.55
35	15-May	33	−61.33	−1.302	−1.501	−1.856	299.3	0.505	689.4	3.542
36	17-May	65	−1262	−30.27	871.4	1.443	1422	6.063	3318	31.34
37	27-May	81	−708.0	−57.50	−56.08	83.73	593.2	11.29	2304	120.4
38	7-Jun	53	−562.6	−7.819	160.0	−12.13	5208	3.245	7040	15.54
39	27-Jun	83	251.6	7.461	−109.3	−158.2	1313	23.49	4927	162.3
40	6 Aug.	130	−2552	−41.87	556.9	−15.92	10832	9.502	17091	123.3
41	13 Aug.	213	−9458	−459.8	582.7	−251.2	6930	14.95	21474	779.3
42	27 Aug.	421	−2351	−182.1	65.95	−208.5	232.9	9.142	4735	562.4
43	16 Sept.	37	−119.0	−3.542	−26.00	−8.022	97.45	0.829	482.9	9.476
44	19 Sept.	76	−234.5	−21.25	13.49	−54.27	101.9	3.192	535.4	63.36
45	14 Oct.	32	−287.1	−6.183	70.01	17.29	76.25	3.866	631.7	21.27
46	20 Oct.	143	−1677	−81.86	291.8	96.15	232.6	8.744	3318	139.6
47	27 Oct.	39	−237.7	−9.271	248.9	67.75	331.1	15.55	1181	71.52
48	31 Oct.	34	−145.5	−1.857	−27.53	−3.215	8041	0.621	15320	5.634
49	3 Nov.	27	−107.1	−1.150	80.51	−0.123	3325	0.238	1901	1.324
50	7 Nov.	26	−122.7	0.062	154.6	33.06	59.79	9.982	431.6	3.498
51	11 Nov.	132	−2086	−269.9	−38.88	−261.5	17032	198.9	26231	2081
Annual totals		**2586**	**−23128**	**−1197**	**4482**	**−1103**	**97905**	**422.5**	**179141**	**5429**

[a]Symbols are defined in the text. B, bed load; S, suspended load.

[23] Wave height time series obtained from buoy 44009 provides information on storm frequency and intensity during periods when the S4s were not deployed. Like the S4s, the buoy was down for maintenance and repair during certain portions of 1994 and 1995. Significant wave height tends to be consistently higher for the buoy. This is due in part because the surface buoy measures waves with wavelengths less than one-half the water depth, which are not sampled by the S4 pressure sensor located near the seabed. During storms, in particular, the higher-frequency locally generated wind waves that contain more energy are sampled by the surface buoy and not the S4 pressure sensor leading to the generally lower wave heights measured at the study site. The NOAA buoy is operational during three major periods when the S4s are not. During September–October 1994, it appears that one major storm occurs that is not included in our data set. For the longer period in April–May 1995, a total of three or four storms were missed. This is about the same number of events identified the previous year during this time period. Finally, it appears that the buoy captured three or four major storms near the end of 1995. This is similar to the number of events identified for this same time period in 1994 when the S4s were deployed. Two other time periods at the end of June and December 1994 also indicate a few storms with sufficient energy to mobilize sediment. Again, they do not seem to be anomalously high compared to seasonal trends as measured by the S4s. Overall, our record, though incomplete, appears to be representative of conditions in terms of both storm frequency and intensity for this 2 year period.

[24] In the vicinity of LEO-15, the New Jersey coastline is oriented approximately 31° clockwise from true north (43° magnetic). The alongshore and cross-shore currents are depicted in Figure 9. For the shore-normal component, positive values denote offshore flow and for the shore-parallel component, positive values denote alongshore flow toward the northeast. Currents are highly variable but during most events they generally show a strong alongshore component that coincides with the timing of the higher waves.

5.1. Sediment Transport Events

[25] Defining the winter storm season as any period between 1 September and 30 April indicates that 32 out of the 51 events (63%) are classified as winter sediment transport events. The longest event begins in August 1995, which is the same period as the sediment transport study that produced the calibrated reference concentration model presented above. The total number of event hours is 4512. Dividing this by the number of hours the S4s were in operation (12751) translates to 35% active sediment mobilization for the recorded time period.

[26] To determine how representative our event criteria is over the 2 year period, plots depicting depth-integrated sediment transport for all time periods are displayed in Figures 10 and 11. For the suspended load, our sediment transport event criteria captures 92% of the total sediment transport for the entire record. For the bed load, only 38% of the total occurs during the identified events. This is due to the fact that the bed load calculation is based on individual waves rather than the equivalent wave, which is a statistical average over many wave periods. Although the statistical representation may indicate that the average wave velocities are too weak to initiate sediment mobilization, the maximum instantaneous wave speed over a given period may exceed the movement threshold. This suggests that moni-

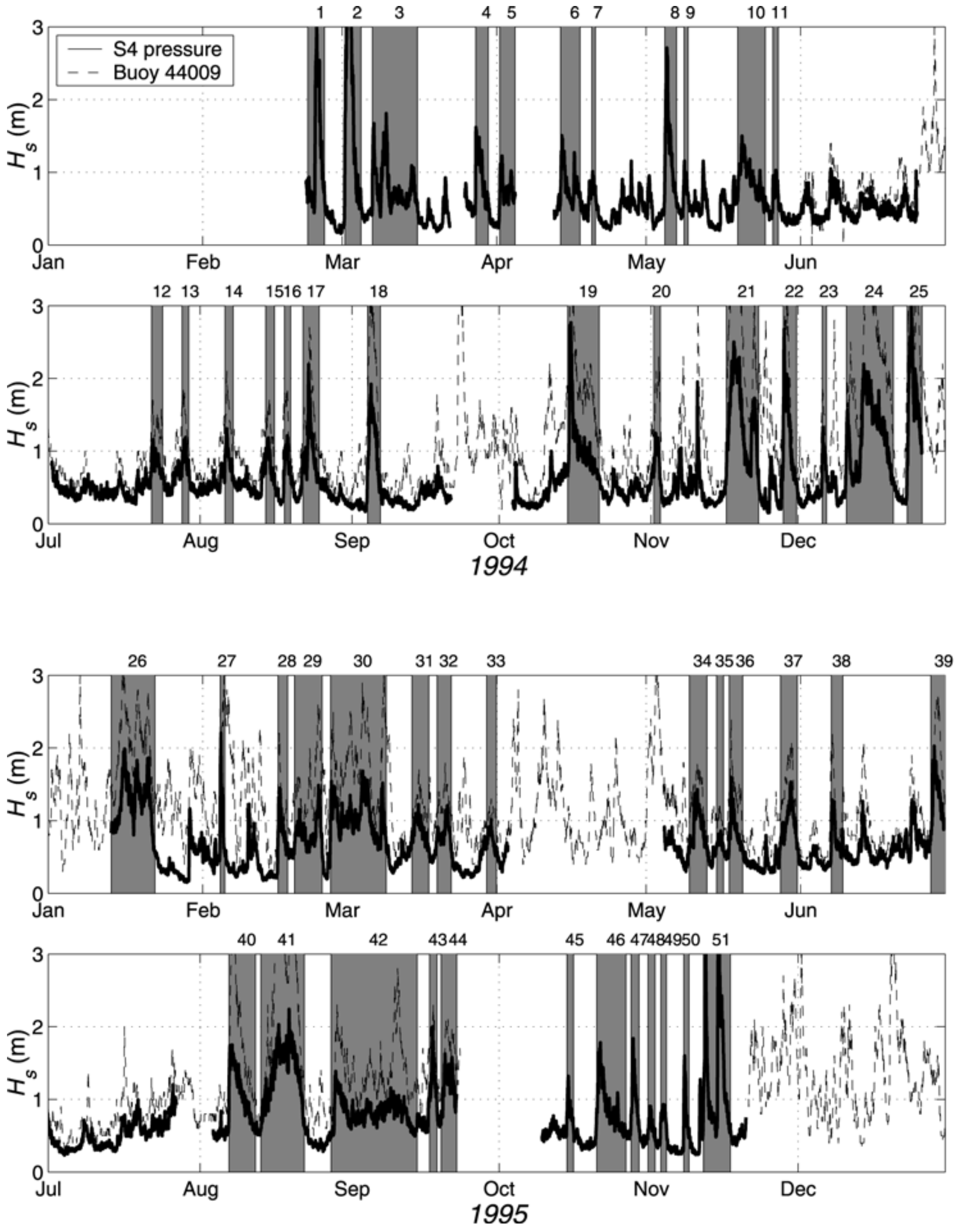

Figure 8. Significant wave height derived from the S4 pressure sensor and NOAA buoy 44009 located near the entrance to Delaware Bay. Shaded regions identify sediment transport events. Numbers above each transport event correspond to the numbering system in Tables 1 and 2.

toring individual waves is as important as storms with strong currents when quantifying interannual sediment transport budgets.

5.2. Cross-Shore and Alongshore Transport

[27] The cross- and alongshore transport for each event is depicted in Figure 12. For the suspended load, the strongest alongshore transport is negative. This dominant southwesterly alongshore component is typical of near-bed current patterns in the MAB during strong northeasters [*Madsen et al.*, 1993; *Wright et al.*, 1994]. The cross-shore component is generally much weaker and more variable.

[28] For nearly all events, the cross- and alongshore bed load transport is greater than the suspended load. There are also more occurrences of alongshore bed load transport directed toward the northeast. The cross-shore component is directed onshore in all but 12 events, which is in agreement with the idea that asymmetries in near-bed wave velocities at LEO-15 drive net sediment transport through ripple migration that is in the direction of the wave [*Traykovski et al.*, 1999]. Overall, the dominant direction associated with the suspended load is alongshore and the dominant direction for the bed load is cross shore.

6. Discussion

6.1. Relationship Between Event Duration, Q_{sm} (Q_{bm}) and Q_{st} (Q_{bt})

[29] Longer events combined with higher waves will lead to larger total depth-integrated sediment transport. The question then arises, Do the longest events result in the greatest transport? A quantitative measure describing the relation-

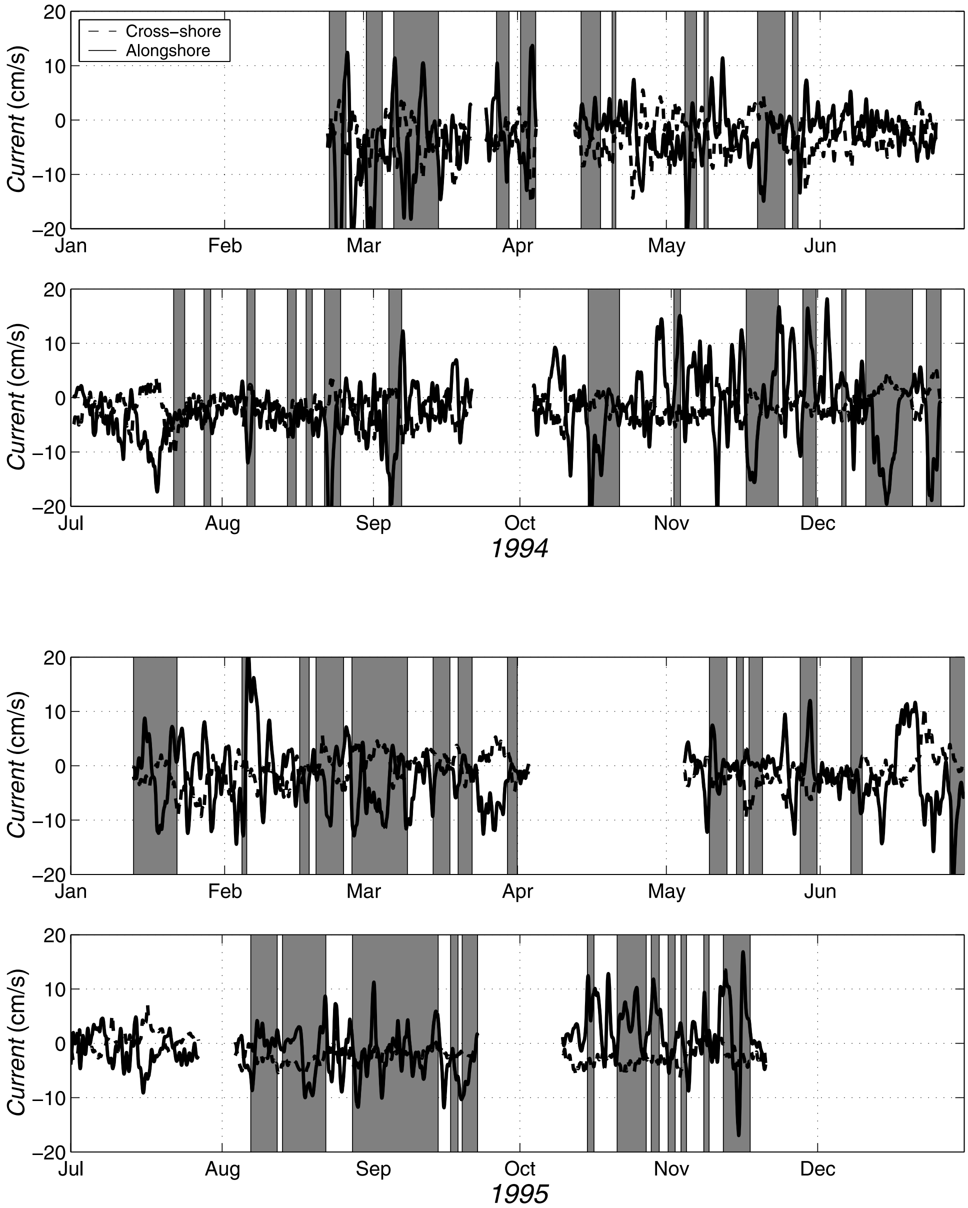

Figure 9. Low-pass-filtered cross- and alongshore currents. The original time series for each component was low-pass filtered with a 36 hour cutoff to remove the tides.

ship between Q_{sm} (Q_{bm}), Q_{st} (Q_{bt}) and event duration is achieved by constructing correlation coefficients representing the normalized covariance between these variables [*Bendat and Piersol*, 1986]. Treating the events as independent observations produces the matrix of correlation coefficients depicted in Table 3. The correlation between Q_{sm} (Q_{bm}) and Q_{st} (Q_{bt}) is high, but none are strongly correlated with event duration. Figure 13 shows suspended sediment transport for events 2 and 51. Although the quantitative features of individual events are unique, these graphs capture the general trend for all events. Within each event, the majority of the transport is confined to a narrow window of intense wave activity. This period is flanked by much longer periods with very low sediment transport. This confinement of the greatest transport around a narrow window independent of temporal scale illustrates why Q_{sm} (Q_{bm}) correlates well with Q_{st} (Q_{bt}) and why event duration does not correlate strongly with either. Although it is still relatively low (29%), the correlation between total transport and event duration is better for bed load than suspended load. Event duration increases in proportion to the number of consecutive hours the skin friction shear stress exceeds the minimum required for the initiation of sediment motion. This, in turn, is proportional to the wave orbital velocity, which is linked to the bed load transport through (4). Therefore it is not too surprising that event duration and Q_{bt} are positively correlated. On the other hand, the suspended load, which shows poorer correlation (16%) between Q_{st} and event duration, is also a function of the current magnitude, which can decay rapidly after a storm while the waves remain fairly large [*Styles and Glenn*, 2002]. Because the currents are even less correlated with

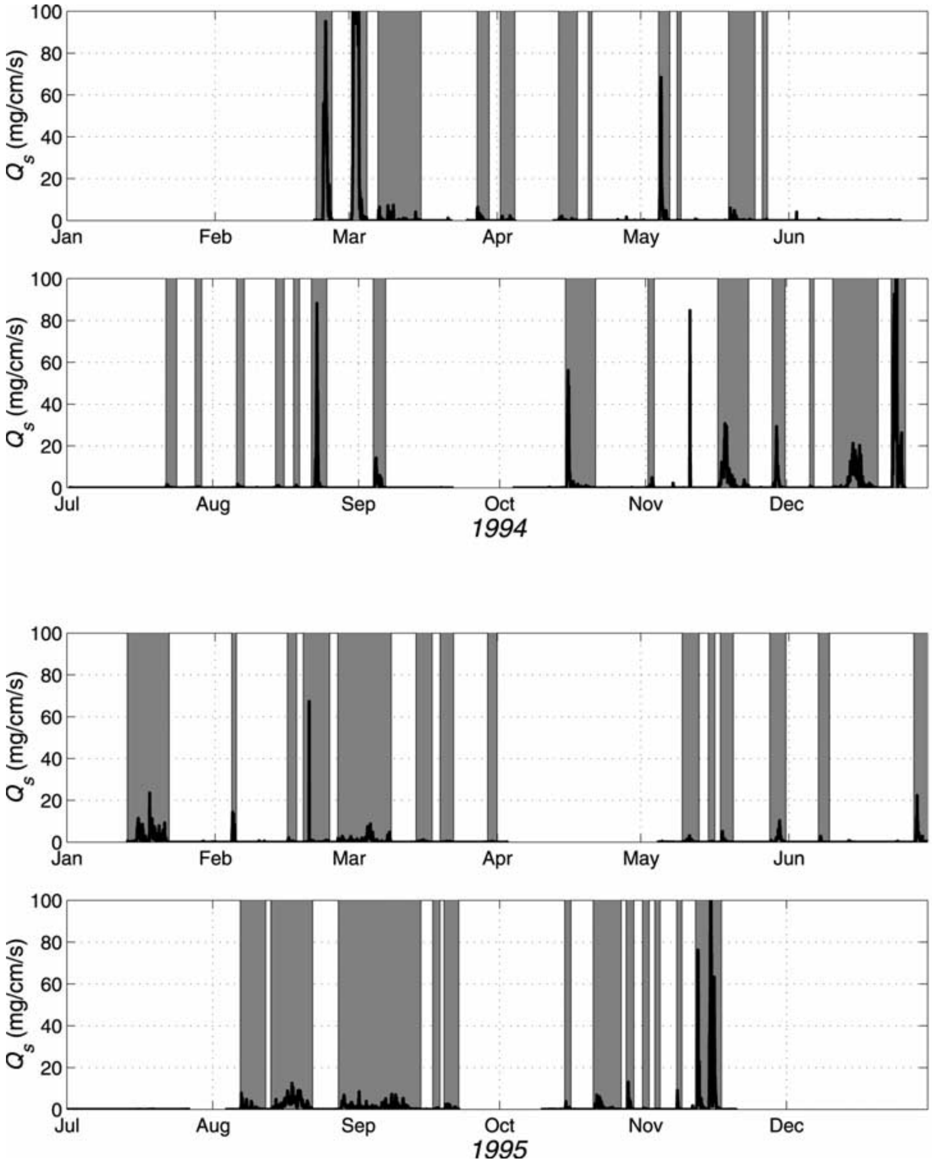

Figure 10. Suspended load transport magnitude for the 2 year time series.

the waves, the correlation coefficient between Q_{st} and event duration is much smaller (5%).

6.2. Seasonal Distributions

[30] In 1994, the total sediment transport is 1.4×10^5 mg/cm and in 1995 it is 1.8×10^5 mg/cm, indicating that 1995 was a slightly more active year. Summer events are defined over a 4 month period (May–August) and account for 37% of the total events. Summertime transport, therefore accounts for a larger fraction than is usually assumed [e.g., *Drake and Cacchione*, 1985]. A few summer storms produced total transport estimates comparable to several moderate winter storms. As an example, the 13 August 1995 event ranked sixth for total suspended load and fourth for total bed load. Net cross-shore transport during the winter is -1.6×10^4 mg/cm and for the summer it is -1.7×10^4 mg/cm. In terms of mode of cross-shore transport, 88% and 96% are contained in the bed load for winter and summer, respectively. Alongshore transport estimates for winter and summer are -3109 mg/cm and 2315 mg/cm, respectively. Forty-nine percent and 74% are contained in the bed load for winter and summer, respectively. Winter events tend to drive sediment transport alongshore toward the southwest and onshore, while summer events drive it alongshore toward the northeast and onshore. The net cross-shore transport is -3.3×10^4 mg/cm and the net alongshore transport is -795 mg/cm. Onshore transport dominates for this 2 year period. If the bed load were neglected, then the total cross- and alongshore transport would be -2990 mg/cm and -1.2×10^4 mg/cm, respectively. Under this latter scenario, the transport is dominated by the alongshore component and it is directed toward the southwest.

6.3. Mechanisms Influencing Cross-Shore Transport

[31] The first-order momentum balance for shelf regions predict offshore flow at the bottom during downwelling and onshore flow during upwelling [*Ekman*, 1905]. Thirty-seven

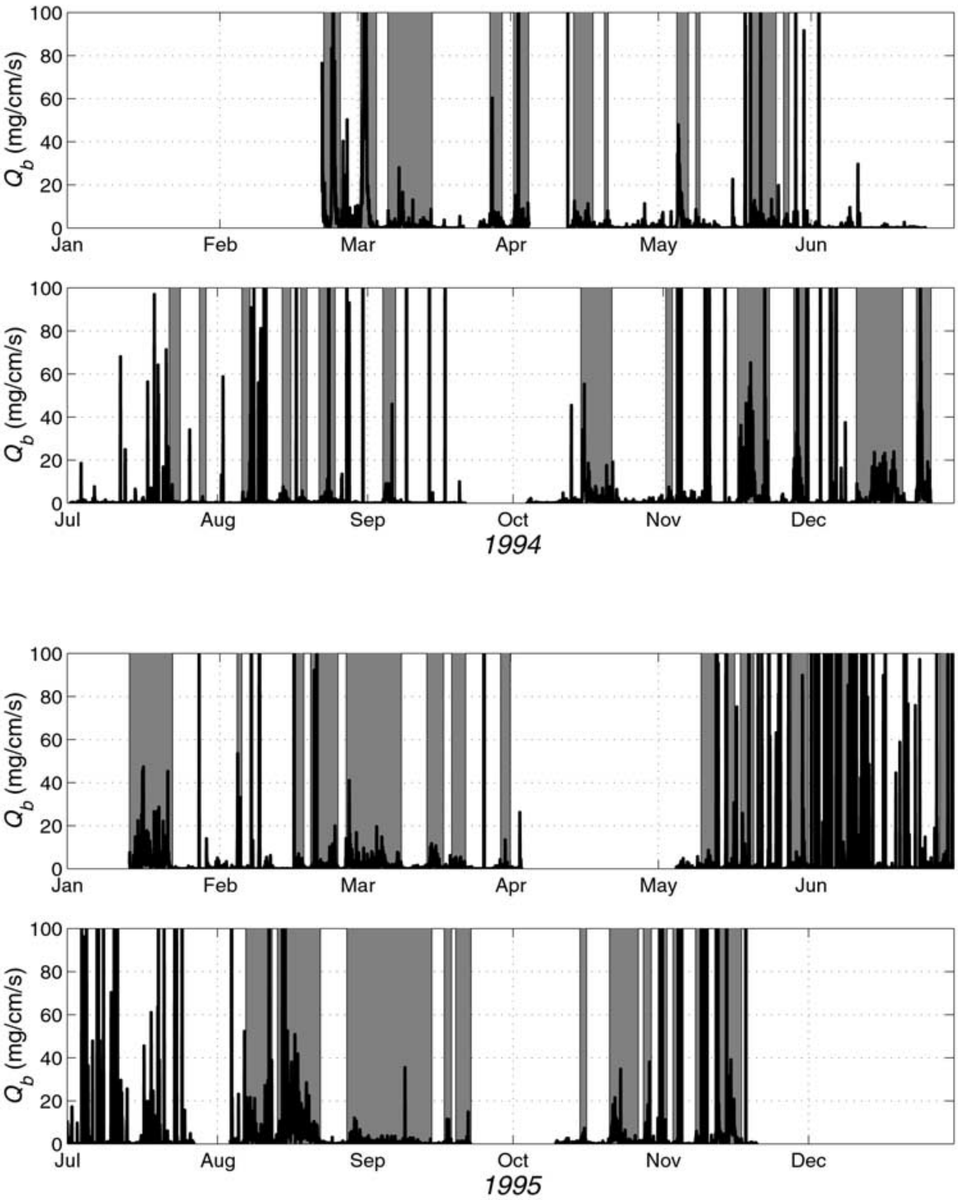

Figure 11. Bed load transport magnitude for the 2 year time series.

of the events indicate alongshore suspended load transport directed toward the southwest. Available alongshore winds are directed toward the southwest during at least some portion of these events (Figure 14). For cases in which the alongshore component switches direction, examination of wave heights indicate that this occurs after the most intense portion of the storm has passed. As an example, event 8 indicates alongshore winds toward the southwest at the very beginning of the event that rotate toward the northeast shortly after the event begins. Because sediment transport is associated with the highest waves, the alongshore suspended sediment transport is greatest while the winds and associated alongshore currents are directed toward the southwest. By the time the winds have shifted, waves heights have decreased and the alongshore suspended sediment transport, which is now directed toward the northeast, is much weaker. This leads to a net transport toward the southwest as indicated in the event integrated results shown in Table 1.

[32] The cross-shore component during periods in which the alongshore wind is toward the southwest varies between onshore and offshore. During events 2, 8, 21, 41, 42, and 51, the cross-shore component is directed onshore. This pattern contradicts the notion of downwelling. The shallow depths at LEO-15 prohibit the full development of Ekman's elementary current system for continental shelves, in which surface and bottom Ekman layers are separated by a geostrophic core interior. Bottom Ekman layer thickness for the MAB during storms has been estimated to be between 10 and 35 m [*Keen and Glenn*, 1995]. This is greater than or equal to the total water depth at LEO-15. Model results for this region have indicated very little current veering during storms in depths less than 20 m [*Keen and Glenn*, 1995]. This is supported by recent

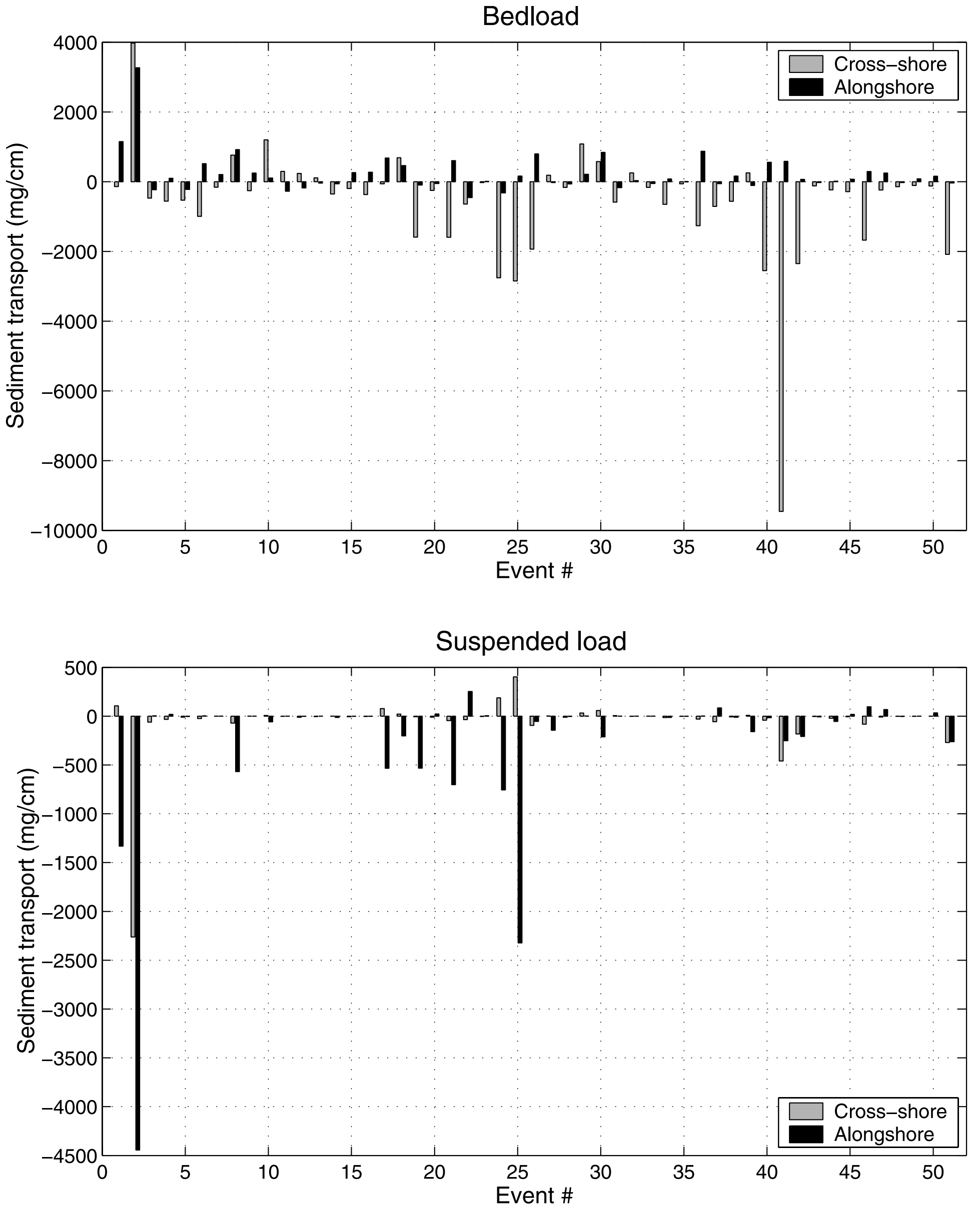

Figure 12. Cross- and alongshore total depth-integrated sediment transport for all 51 events. Negative values denote alongshore flow toward the southwest and cross-shore flow onshore. Numerical values are listed in Tables 1 and 2.

observations that indicate less veering during the well-mixed winter season [*Kohut et al.*, 2004]. Also, the wind correlated component of surface currents tend to be to the left of the wind direction [*Kohut et al.*, 2004]. This supports the consistent onshore bottom current during the second event, which is accompanied by a strong onshore wind component during the period with highest waves. For the eighth event, the cross-shore current is nearly zero during the period of highest waves, which results in little cross-shore transport. Near the end of the event, the cross-shore current is onshore and is accompanied by an offshore wind. The alongshore wind component also switches direction in the middle of the event. This event occurs in mid-May when surface heating is more than likely stratifying the water column. For a stratified water column, *Münchow and Chant* [2000] noted significant veering and *Kohut et al.* [2004] noted that the ocean response is more consistent with upwelling/downwelling. Event 41 is also during the summer stratified season and the wind and responding currents are consistent with upwelling/downwelling. It is important to note that for events 21 and 42, the cross-shore bottom current tends to be weak or slightly onshore during the majority of the time regardless of wind direction. This

Table 3. Correlation Between Maximum Depth-Integrated Concentration, Total Depth-Integrated Concentration, and Event Duration

	Suspended Load, %	Bed Load, %
Total/maximum	96	93
Total/duration	16	29
Maximum/duration	5	8

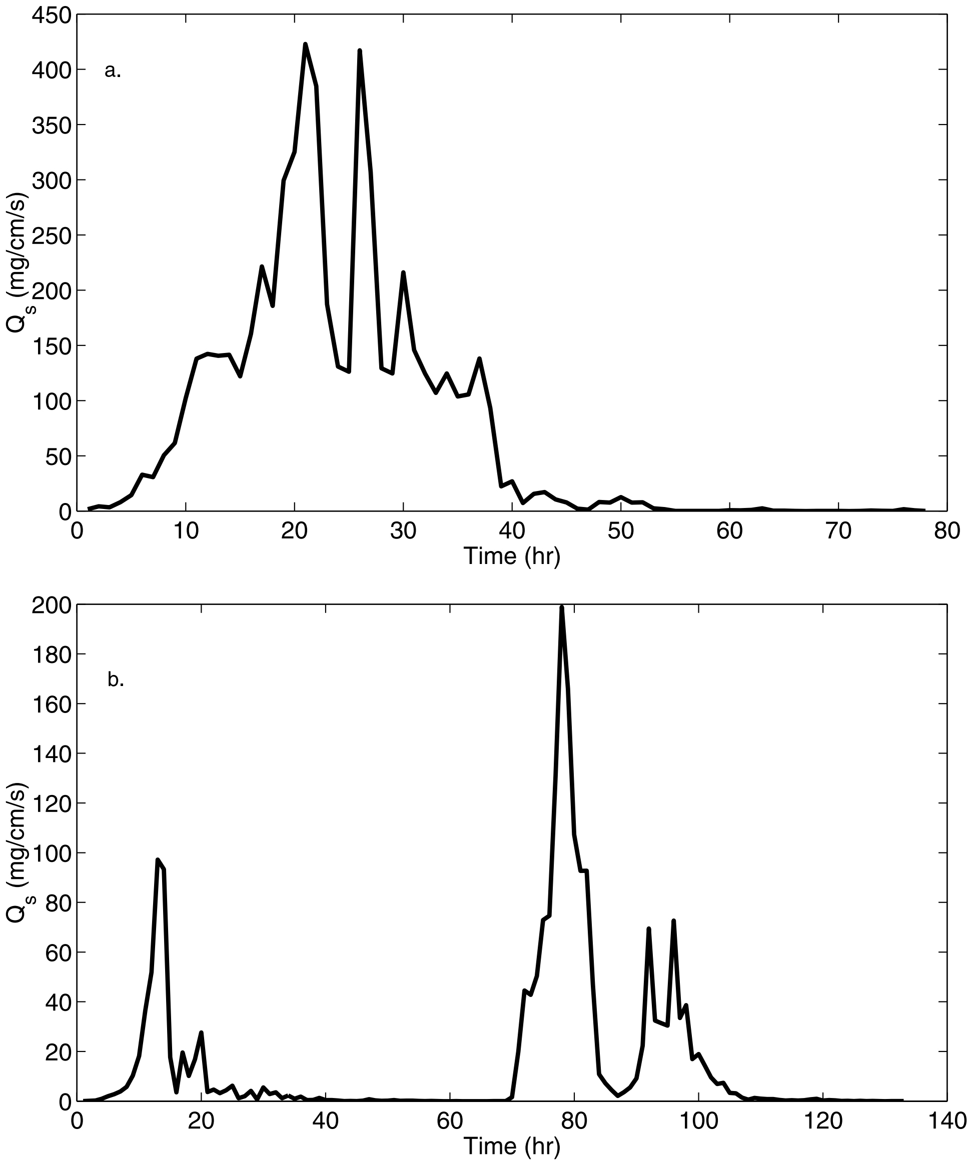

Figure 13. Time series of the magnitude of the depth-integrated suspended sediment transport for the (a) 2nd and (b) 51st events.

persistent onshore component may be attributed to a combination of wind forcing and local bathymetry. The S4s were placed at the southern end of a shore-oblique sand ridge. Previous work has indicated that cross-shore currents in the trough of these ridges tends to be slightly onshore [*Trowbridge*, 1995], which is consistent with our observations. *Kohut et al.* [2004] have also noted the importance of bathymetry in controlling current direction when the water column is well mixed. For the 51st event, wind data is not available, but it is suspected that the response should be consistent with other wintertime events.

[33] The majority of the cross-shore bed load transport is directed onshore. This is in agreement with the generation of higher orbital velocities during the forward half of the wave cycle typical of slightly nonlinear waves over rippled beds [*Davies and Villaret*, 1998]. The magnitude of the onshore transport also increases in proportion to wavelength (Figure 15). Longer waves generally will produce higher orbital velocities and associated sediment transport [*Wright et al.*, 1994]. During 12 of the events, the bed load transport is directed offshore. A bimodal spectrum consisting of local sea waves and swell has been shown to produce negatively skewed orbital velocities that result in offshore ripple migration [*Crawford and Hay*, 2003]. Analysis of the wave energy spectrum during the second event reveals a bimodal character and associated negative skewness surrounding the most intense period of bed load transport (Figure 16). Negative skewness is associated with all events that possess offshore transport. The bimodal character illustrated in Figure 16 is also prominent during at least some portion of these other events.

6.4. Comparison to Previous Studies

[34] For the suspended load, we found that 63% of the events occurred during the winter storm season. For a similar study from the west coast of the United States,

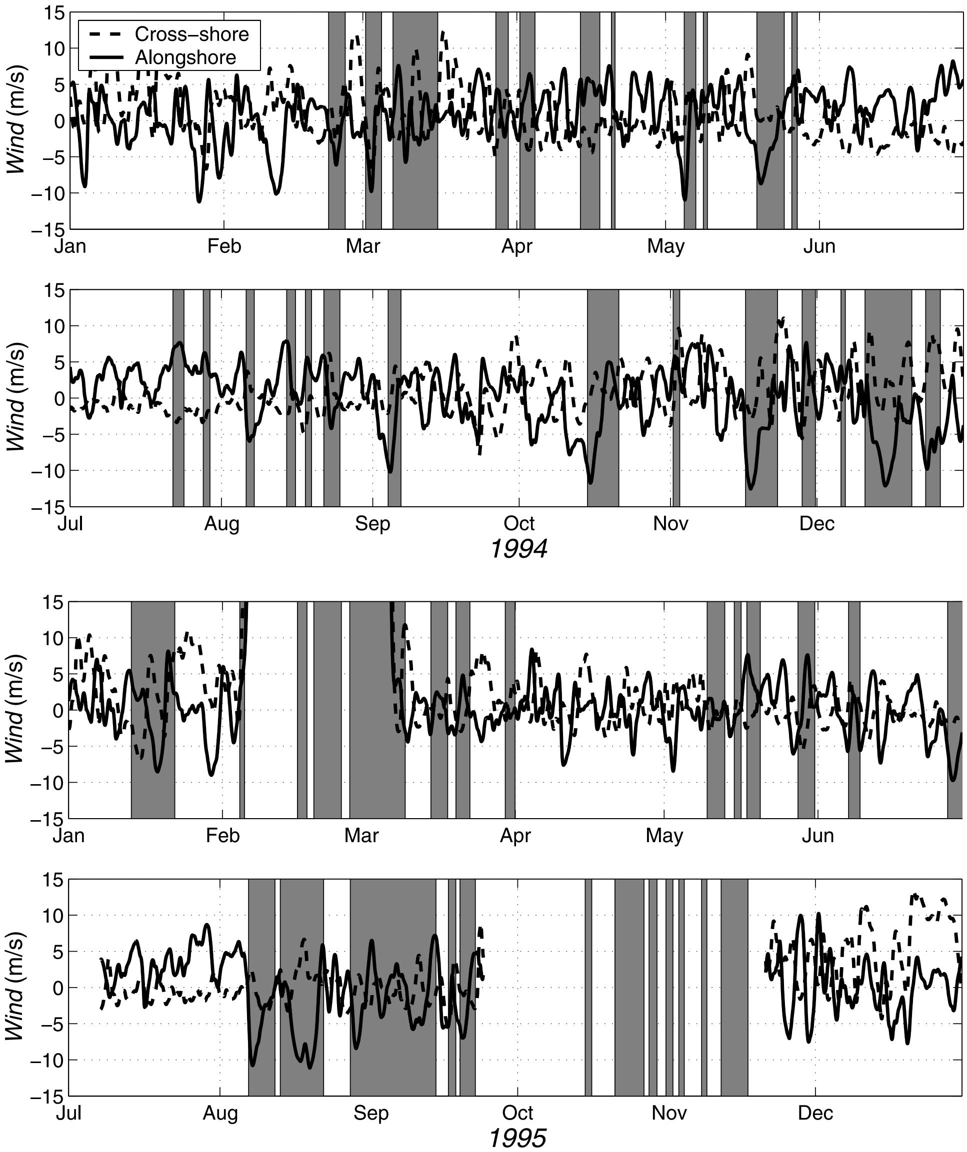

Figure 14. Time series of low-passed-filtered cross- and alongshore wind obtained from NOAA buoy 44009.

Ogstron and Sternberg [1999] found 85% of the transport events occurred in the winter. This difference is partially due to the varied criteria used to define a sediment transport event. The present study defines a sediment transport event in terms of event duration, whereas *Ogstron and Sternberg* [1999] defined a transport event in terms of a minimal concentration at a given height above the bottom. Because winter sediment transport events tend to be stronger in terms of sediment concentrations, it is likely that *Ogstron and Sternberg* [1999] find a higher percentage of events in the winter that exceed their event criteria threshold. *Ogstron and Sternberg* [1999] identified 41 sediment transport events in 1 year, which is greater than the average 25 that we identified over a 2 year period. Again, the differences are likely attributed to the fact that they include shorter events that do not satisfy the event criteria threshold established in the present study. A single winter storm in March 1994 accounts for 51% of the total suspended sediment transport for that year. That a single winter storm can be responsible for the majority of the annual transport appears to be a common feature of sediment transport patterns in other continental shelf environments [*Ogstron and Sternberg*, 1999].

[35] Most of the previous studies conducted on the northern California, Washington or Oregon shelf were in 35–130 m of water. A combination of local waves, swell, tidal and wind driven currents, and river discharge drive sediment transport in this region [*Drake and Cacchione*, 1985; *Ogstron and Sternberg*, 1999; *Ogstron et al.*, 2000; *Sherwood et al.*, 1994; *Traykovski et al.*, 2000]. Unlike LEO-15 these shelf regions are narrower, steeper and generally contain finer bed material including midshelf mud patches [*Sherwood et al.*, 1994; *Traykovski et al.*, 2000]. On the northern California shelf sediment transport is linked to local storm events, but a significant fraction have been known to be driven by distance swell coupled with local currents. *Sherwood et al.* [1994] found net transport to be primarily directed offshore and toward the

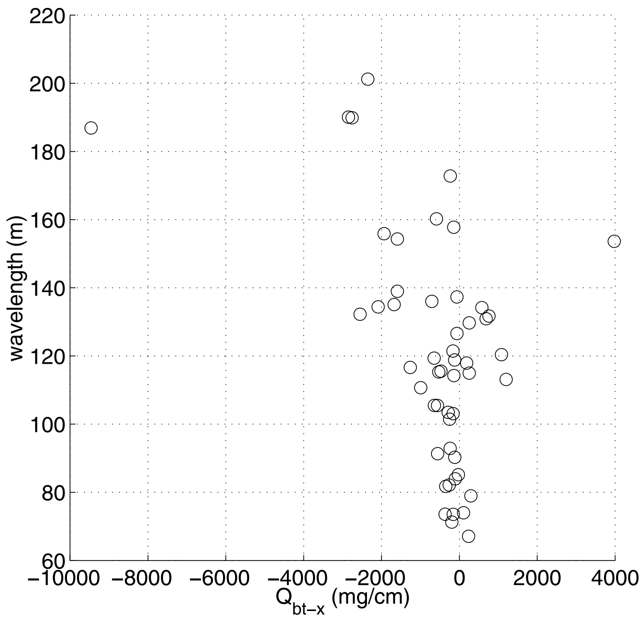

Figure 15. Scatterplot depicting the general increase in cross-shelf bed load transport with wavelength. Negative values denote onshore transport.

north, in agreement with southerly winds that drive downwelling and alongshore transport. *Ogstron and Sternberg* [1999] also noted offshore transport on the northern California shelf but the net alongshore component was directed toward the south.

[36] At our shallow water site (10 m depth), suspended sediment transport is tied strongly to the wind and waves, but alongshore winds with even a weak cross-shore component can lead to transport patterns that cannot be interpreted in terms of Ekman's classic elementary current system for continental shelves. Recent results have indicated, rather, that during the well-mixed winter storm season the water column responds as a single frictional layer with little current veering [*Kohut et al.*, 2004]. Under these conditions, topography as well as local wind direction plays an important role in determining current direction and, therefore, associated suspended sediment transport.

[37] *Lyne et al.* [1990] analyzed results from five tripods to examine sediment transport during the 1979–1980 winter storm season at selected locations within the MAB. Their southern most station was in 63 m of water located offshore of the LEO-15 site. A comparison between their results and ours provides some insight into cross-shore variability for the New Jersey shelf. From their estimates of sediment transport, it appears as if five major events occurred between December 1979 and April 1980. For the equivalent time period in 1994 and 1995 we identify nine and eight events, respectively. The larger number of events may be related to the fact that our site is much shallower and therefore experiences more frequent energetic waves that may not penetrate to 63 m depth. Net transport computed by *Lyne et al.* [1990] was directed primarily along the shelf toward the south. This is consistent with our results during the winter storm season, in which northeasters generate significant bottom currents toward the south along isobaths at LEO-15. *Harris et al.* [2003] examined sediment transport in the nearby Hudson Shelf Valley located northeast of the LEO-15 study site. In contrast to the alongshore suspended sediment transport indicative of our study site, the transport within the Hudson Shelf Valley was directed primarily along its generally shore normal axis. Therefore transport within the valley is constrained by the bathymetry and associated complex circulation patterns apparent to this region [*Harris et al.*, 2003].

[38] The above findings for the LEO-15 site are consistent with the sediment transport model results for the MAB overall [*Keen and Glenn*, 1995]. *Keen and Glenn* [1995] noted that the storm driven bottom currents were generally weaker than tidal currents. This produced an interesting flow pattern in which downwelling conditions coupled with an ebbing tide increased current veering in the bottom boundary layer driving sediment transport offshore. During flood, bottom currents realigned themselves in the alongshore direction consistent with the wind patterns associated with the northeaster they modeled. Our current measurements, however, indicate significant alongshore bottom currents during storms regardless of tidal phase. This is likely due to the fact that our measurements are taken in 10 m of water, which represents the landward boundary of the *Keen and Glenn* [1995] model. However, it does suggest that cross-shore variability and the interaction of tidal currents for regions seaward of LEO-15 should be taken into account when trying to assess shelf-wide transport budgets.

[39] Unlike the above mentioned studies of long-term sediment transport, bed load transport was explicitly included in the calculations presented here. It was found that wave-forced bed load accounts for a significant fraction of the total, and should be included in future model estimates of sediment budgets for inner shelf regions where waves are strongest.

7. Summary

[40] Nearly 2 years of wave and current measurements obtained on the inner New Jersey shelf and a model have furnished a glimpse into processes driving long-term sediment mobility at LEO-15. Common to all sediment transport events was an unmistakable dominance by waves in initiating and maintaining sediment mobility. Total transport was highly correlated with maximum depth integrated transport, with event duration relatively weak by comparison. The most energetic transport events occurred during the winter storm season. Summer storms, however, contributed significantly to the overall transport budget, with several summer transport events comparable in magnitude to moderate winter events.

[41] Suspended sediment transport was directed primarily alongshore and wave-forced bed load was directed primarily cross shore. In most cases, cross-shore suspended sediment transport followed expected patterns typical of the inner shelf with onshore (offshore) transport associated with upwelling (downwelling). Noted exceptions occurred in which alongshore winds toward the southwest were accompanied by onshore transport near the seabed. During most transport events, bed load was primarily onshore due to wave asymmetries that produce higher orbital velocities during the forward half of the wave cycle. At other times

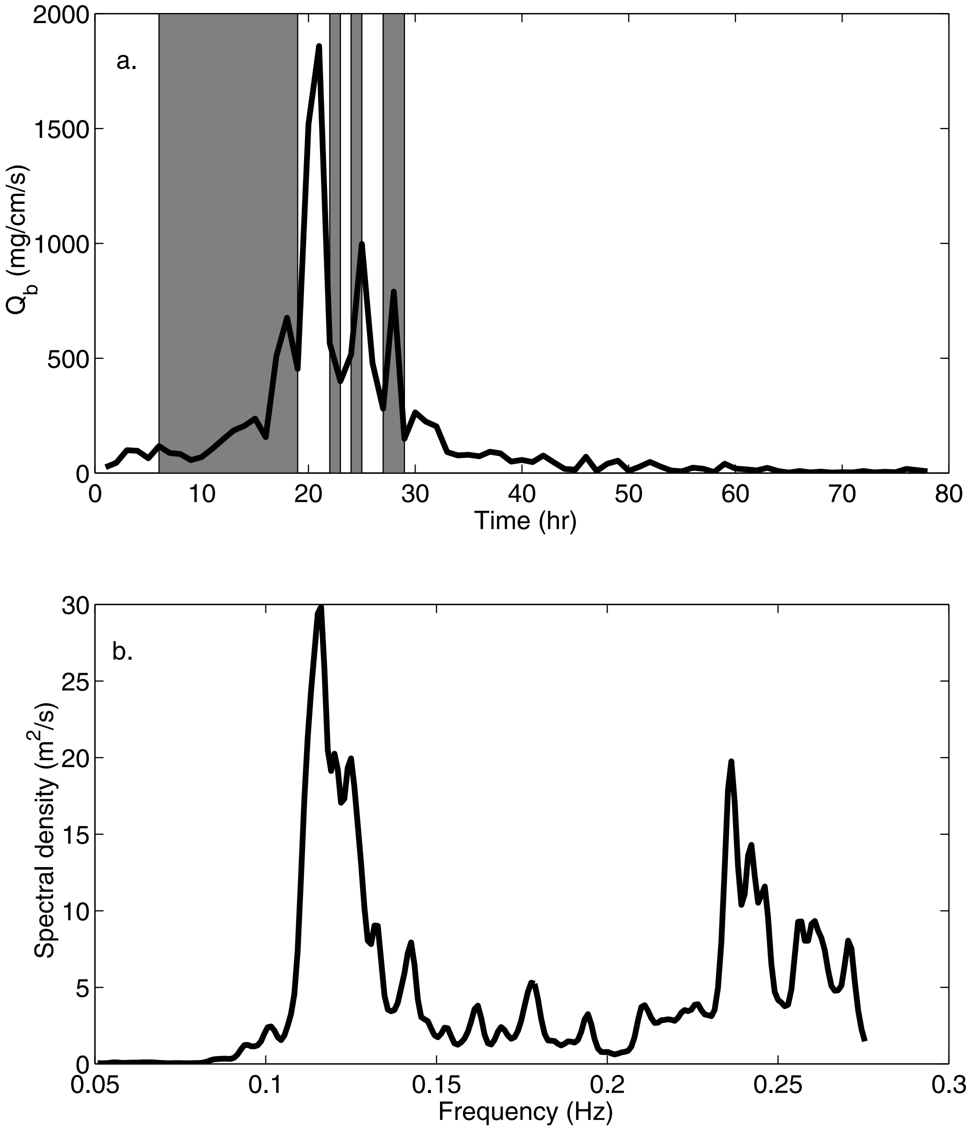

Figure 16. (a) Time series of the magnitude of the bed load transport during the second event. Shaded regions identify periods when the wave spectral density function is bimodal. (b) Spectral density function obtained from the 18 min burst during hour 10 of the second event, illustrating the bimodal character.

bed load transport was directed offshore due to reversals in wave asymmetry associated with a bimodal wave spectrum. Overall, the transport budget for the 2 year period was alongshore toward the southwest and slightly onshore.

[42] Our choice to separate the transport into bed load and suspended load contributions has indicated that wave-forced bed load is the dominant mode. This is especially true for the cross-shore transport. Therefore bed load should be included in future calculations of sediment transport in high-energy continental shelf environments.

[43] **Acknowledgments.** The authors would like to thank James Irish, James Lynch, and Peter Traykovski of the Woods Hole Oceanographic Institution for providing the suspended sediment concentration data used to calibrate the model. We also want to thank Elizabeth Creed, Rose Petrecca, John Zlotnik, and the staff of the Rutgers University Marine Field Station for deploying, servicing, and maintaining the S4s. Insightful comments from two anonymous reviewers and the Associate Editor are greatly appreciated. This work was supported by the Coastal Ocean Modeling and Observation Program (N00014-97-1-0797) and the National Ocean Partnership Program (N00014-97-1-1019 and N00014-98-1-0815). We also acknowledge the continued support of the MAB National Oceanographic and Atmospheric Administration/National Undersea Research Program (MAB 96-10, NYB 94-7, and NA06RU0139). Partial funding for the first author was also provided by the SouthEast Atlantic Coastal Ocean Observing System (SEACOOS).

References

Atkinson, K. E. (1989), *An Introduction to Numerical Analysis*, 693 pp., John Wiley, Hoboken, N. J.

Bendat, J. S., and A. G. Piersol (1986), *Random Data, Analysis and Measurement Procedures*, 566 pp., Wiley-Interscience, Hoboken, N. J.

Cacchione, D. A., W. D. Grant, D. E. Drake, and S. M. Glenn (1987), Storm-dominated bottom boundary layer dynamics on the northern California continental shelf: Measurements and predictions, *J. Geophys. Res.*, *92*, 1817–1827.

Crawford, A. M., and A. E. Hay (2003), Wave orbital velocity skewness and linear transition ripple migration: Comparison with weakly nonlinear theory, *J. Geophys. Res.*, *108*(C3), 3091, doi:10.1029/2001JC001254.

Davies, A. G., and C. Villaret (1998), Wave-induced currents above a rippled bed, in *Physics of Estuaries and Coastal Seas*, edited by J. Dronkers and M. B. A. M. Cheffers, pp. 187–199, A. A. Balkema, Brookfield, Vt.

Drake, D. E., and D. A. Cacchione (1985), Seasonal variation in sediment transport on the Russian River shelf, California, *Cont. Shelf Res.*, *4*, 495–514.

Ekman, V. W. (1905), On the influence of the Earth's rotation on ocean currents, *Ark. Mat. Astron. Fys.*, *2*, 1–53.

Glenn, S. M., and W. D. Grant (1987), A suspended sediment correction for combined wave and current flows, *J. Geophys. Res.*, *92*, 8244–8246.

Glenn, S. M., T. D. Dickey, B. Parker, and W. Boicourt (2000), Long-term real-time coastal ocean observation networks, *Oceanography*, *13*, 24–34.

Grant, W. D., and O. S. Madsen (1979), Combined wave and current interaction with a rough bottom, *J. Geophys. Res.*, *89*, 1797–1808.

Grant, W. D., and O. S. Madsen (1982), Movable bed roughness in unsteady oscillatory flow, *J. Geophys. Res.*, *87*, 469–481.

Grant, W. D., and O. S. Madsen (1986), The continental-shelf bottom boundary layer, *Annu. Rev. Fluid Mech.*, *18*, 265–305.

Harris, C. K., and P. L. Wiberg (1997), Approaches to quantifying long-term continental shelf sediment transport with an example from the northern California STRESS mid-shelf site, *Cont. Shelf Res.*, *17*, 1389–1418.

Harris, C. K., B. Butman, and P. Traykovski (2003), Winter-time circulation and sediment transport in the Hudson Shelf Valley, *Cont. Shelf Res.*, *23*, 801–820.

Keen, T. R., and S. M. Glenn (1995), A coupled hydrodynamic-bottom boundary layer model of storm and tidal flow in the Middle Atlantic Bight of North America, *J. Phys. Oceanogr.*, *25*, 391–406.

Kohut, J. T., S. M. Glenn, and R. J. Chant (2004), Seasonal current variability on the New Jersey inner shelf, *J. Geophys. Res.*, *109*, C07S07, doi:10.1029/2003JC001963.

Lyne, V. D., B. Butman, and W. D. Grant (1990), Sediment movement along the U.S. east coast continental shelf, II. Modeling suspended sediment concentration and transport rate during storms, *Cont. Shelf Res.*, *10*, 429–460.

Madsen, O. S. (1994), Spectral wave-current bottom boundary layer flows, in *Proceedings of the 24th Coastal Engineering Conference*, pp. 384–398, Am. Soc. of Civ. Eng., Washington, D. C.

Madsen, O. S., and P. N. Wikramanayake (1991), Simple models for turbulent wave-current bottom boundary layer flow, *Contract Rep. DRP-91-1*, U.S. Army Corps of Eng. Coastal Eng. Res. Cent., Vicksburg, Miss.

Madsen, O. S., Y.-K. Poon, and H. C. Graber (1988), Spectral wave attenuation by bottom friction: Theory, in *Proceedings of the 21st Coastal Engineering Conference*, pp. 491–504, Am. Soc. of Civ. Eng., Washington, D. C.

Madsen, O. S., L. D. Wright, J. D. Boon, and T. A. Chisholm (1993), Wind stress, bed roughness and sediment suspension on the inner shelf during an extreme storm event, *Cont. Shelf Res.*, *13*, 1303–1324.

Mathisen, P. P., and O. S. Madsen (1996a), Waves and currents over a fixed rippled bed: 1. Bottom roughness experienced by waves in the presence and absence of currents, *J. Geophys. Res.*, *101*, 16,533–16,542.

Mathisen, P. P., and O. S. Madsen (1996b), Waves and currents over a fixed rippled bed: 2. Bottom and apparent roughness experienced by currents in the presence of waves, *J. Geophys. Res.*, *101*, 16,543–16,550.

McClennen, C. E. (1973), Sands on continental shelf off New Jersey move in response to waves and currents, *Maritimes*, *17*, 14–16.

Münchow, A., and R. Chant (2000), Kinematics of inner shelf motions during the summer stratified season off New Jersey, *J. Phys. Oceanogr.*, *30*, 247–268.

Ogstron, A. S., and R. W. Sternberg (1999), Sediment-transport events on the northern California continental shelf, *Mar. Geol.*, *154*, 69–82.

Ogstron, A. S., D. A. Cacchione, R. W. Sternberg, and G. C. Kineke (2000), Observations of storm and river flood-driven sediment transport to the northern California continental shelf, *Cont. Shelf Res.*, *20*, 2141–2162.

Sherwood, C. R., B. Butman, D. A. Cacchione, D. E. Drake, T. F. Gross, R. W. Sternberg, P. L. Wiberg, and A. J. Williams III (1994), Sediment transport events on the northern California continental shelf during the 1990–1991 STRESS experiment, *Cont. Shelf Res.*, *14*, 1063–1099.

Smith, J. D. (1977), Modeling of sediment transport on continental shelves, in *The Sea*, vol. 6, edited by E. D. Goldberg et al., pp. 538–577, Wiley-Interscience, Hoboken, N. J.

Smith, J. D., and S. R. McLean (1977), Spatially averaged flow over a wavy surface, *J. Geophys. Res.*, *82*, 1735–1746.

Styles, R., and S. M. Glenn (2000), Modeling stratified wave and current bottom boundary layers on the continental shelf, *J. Geophys. Res.*, *105*, 24,119–24,139.

Styles, R., and S. M. Glenn (2002), Modeling bottom roughness in the presence of wave-generated ripples, *J. Geophys. Res.*, *107*(C8), 3110, doi:10.1029/2001JC000864.

Swift, D. J. P., and M. E. Field (1981), Evolution of a classic sand ridge field: Maryland Sector, North American inner shelf, *Sedimentology*, *28*, 461–482.

Traykovski, P., A. E. Hay, J. D. Irish, and J. F. Lynch (1999), Geometry, migration, and evolution of wave orbital ripples and LEO-15, *J. Geophys. Res.*, *104*, 1505–1524.

Traykovski, P., W. R. Geyer, J. D. Irish, and J. F. Lynch (2000), The role of wave-induced density-driven fluid mud flows for cross-shelf transport to the Eel River continental shelf, *Cont. Shelf Res.*, *20*, 2113–2140.

Trowbridge, J. H. (1995), A mechanism for the formation and maintenance of shore-oblique sand ridges on storm-dominated shelves, *J. Geophys. Res.*, *100*, 16,071–16,086.

von Alt, C. J., and J. F. Grassle (1992), LEO-15: An unmanned long term environmental observatory, *Proc. Oceans*, *92*, 849–854.

Wiberg, P., and J. D. Smith (1983), A comparison of field data and theoretical models for wave-current interactions at the bed on the continental shelf, *Cont. Shelf Res.*, *2*, 147–162.

Wikramanayake, P. N., and O. S. Madsen (1992), Calculation of suspended sediment transport by combined wave-current flows, *Contract Rep. DRP-92*, 148 pp., U.S. Army Corps of Eng. Coastal Waterw. Res. Cent., Vicksburg, Miss.

Wright, L. D., J. D. Boon, S. C. Kim, and J. H. List (1991), Modes of cross-shore sediment transport on the shoreface of the Middle Atlantic Bight, *Mar. Geol.*, *96*, 19–51.

Wright, L. D., J. P. Xu, and O. S. Madsen (1994), Across-shelf benthic transports on the inner shelf of the Middle Atlantic Bight during the "Halloween storm" of 1991, *Mar. Geol.*, *118*, 61–77.

S. M. Glenn, Coastal Ocean Observation Laboratory, Institute of Marine and Coastal Sciences, Rutgers University, New Brunswick, NJ 08903, USA. (glenn@imcs.rutgers.edu)

R. Styles, Department of Geological Sciences, University of South Carolina, Columbia, SC 29208, USA. (rstyles@geol.sc.edu)